EFFECT OF CHROMIUM ON THE OXIDATION OF STEELS USED IN
THE CONSTRUCTION OF PETROLEUM REFINERY HEATERS

A THESIS SUBMITTED TO
THE GRADUATE SCHOOL OF NATURAL AND APPLIEDSCIENCES
OF
MIDDLE EAST TECHNICAL UNIVERSITY

BY

ABDELRAHMAN SALEH SULTAN

IN PARTIAL FULFILLMENT OF THE REQUIREMENTS FOR
THE DEGREE OF DOCTOR OF PHILOSOPHY

IN

METALLURGICAL AND MATERIALS ENGINEERING

SEPTEMBER 2013

Approval of the thesis:

EFFECT OF CHROMIUM ON THE OXIDATION OF STEELS USED IN THE CONSTRUCTION OF PETROLEUM REFINERY HEATERS

Submitted by **ABDELRAHMAN SULTAN** in partial fulfillment of the requirements for the degree of **Doctor of Philosophy in Metallurgical and Materials Engineering Department, Middle East Technical University, Ankara - Turkey** by,

Prof. Dr. Canan Özgen _____
Dean**,** Graduate School of **Natural and Applied Sciences**

Prof. Dr. C.Hakan Gur _____
Head of Department, **Metallurgical and Materials Engineering**

Prof. Dr. Ishak Karakaya _____
Supervisor, **Metallurgical and Materials Engineering Dept., METU**

Examining Committee Members:

Prof. Dr. C.Hakan Gur _____
Metallurgical and Materials Engineering Dept., METU

Prof. Dr. Ishak Karakaya _____
Metallurgical and Materials Engineering Dept., METU

Prof. Dr. Naci Sevinç _____
Metallurgical and Materials Engineering Dept., ATILIM Uni.

Assist. Prof. Dr. Yener Kuru _____
Metallurgical and Materials Engineering Dept., METU

Assist. Prof. Dr Erkan Konca _____
Metallurgical and Materials Engineering Dept., ATILIM Uni.

Date: 04.09.2013

I hereby declare that all information in this document has been obtained and presented in accordance with academic rules and ethical conduct. I also declare that, as required by these rules and conduct, I have fully cited and referenced all material and results that are not original to this work.

Name, Last name: Abdelrahman Sultan

Signature:

ABSTRACT

EFFECT OF CHROMIUM ON THE OXIDATION OF STEELS USED IN THE CONSTRUCTION OF PETROLEUM REFINERY HEATERS

Sultan, Abdelrahman

Ph.D., Department of Metallurgical and Materials Engineering

Supervisor: Prof. Dr. İshak Karakaya

September 2013, 77 pages

Low chromium steels used in the construction of petroleum refinery heaters work in flue gas environments containing water vapor. On the other hand, the higher oxidation rates of chromium containing steels in moist atmospheres have been reported. P-5, P-22, P-11(containing 5, 2.25 and 1.25 %Cr) and C-5 steels, used in petroleum refinery construction, were subjected to isothermal oxidation tests. These steels were tested in two different environments; air and flue gas of natural gas combustion -$CO_2+2H_2O+7.52N_2$ gas mixture- by using a thermogravimetric analysis (TGA) technique. They were tested at 450 and 500°C to cover the temperature range used in the operation of heaters. From the analysis it was found that P-5 steel retained the best oxidation resistance among all steels in air while in $CO_2+N_2+H_2O$ environment, C-5 was superior to P-5 and P-22. To analyze the oxides and to correlate the TGA results to oxide composition and morphology; optical microscopy, SEM-EDX examinations and XRD measurement were performed. The lower oxidation rates of P-5 and P-22 steels in air were explained with reference to an oxide layer with higher chromium at the surface. On the other hand, the higher oxidation rate in $CO_2+2H_2O+7.52N_2$, was explained by the loss of the protective property of the oxide due to internal oxidation of chromium. The higher corrosivity of water vapor containing environments on Cr containing steels was attributed to the increase in permeability of oxidants to steel due to expansion of lattice parameters by dissolution of hydrogen which was formed by the combustion reaction and/or decomposition of water vapor. It was shown that addition of free oxygen to H_2O containing environments reduces the rate of oxidation. R value representing the ratio of H_2O to O_2 mole fraction was found to be an important parameter to determine the behavior of Cr containing steels in moist atmosphere in the presence of free oxygen.

Keywords: Chromium steels, High temperature, hydrogen, internal oxidation, petroleum refinery heaters, thermogravimetric analysis, water vapor

ÖZ

PETROL RAFİNERİSİ ISITICILARININ YAPIMINDA KULLANILAN ÇELİKLERİN OKSİTLENMELERİNDE KROMUN ETKİSİ

Sultan, Abdelrahman

Doktora, Metalurji ve Malzeme Mühendisliği Bölümü

Tez Yöneticisi: Prof. Dr. İshak Karakaya

Eylül 2013, 77 sayfa

Petrol rafinerisi ısıtıcılarının yapımında kullanılan düşük kromlu çelikler, su buharı içeren baca gazı ortamında çalışırlar. Öte yandan, krom içeren çeliklerin su buharı ortamında daha yüksek oksitlenme hızına sahip oldukları bildirilmiş durumdadır. Petrol rafinerisi yapımında kullanılan, (P-5, P-22, P-11 (%5, 2.25 ve 1.25 Cr içeren) ve C5 çelikleri sabit sıcaklık oksitlenme testlerine tabi tutulmuşlardır. Söz konusu çelikler termogravimetrik analiz tekniği (TGA) kullanılarak iki farklı ortamda test edilmişlerdir: hava ve doğal gazın yanması sonucu oluşan gaz kompozisyonu, $CO_2+2H_2O+7.52N_2$. Çelikler, ısıtıcıların çalıştığı sıcaklık aralığını kapsayacak şekilde 450 ve 500°C'lerde test edilmişlerdir. Analizlerden, P-5 çeliğinin, havada, tüm çelikler arasında en iyi dirence sahip olduğu; bununla beraber $CO_2+N_2+H_2O$ ortamında, C5'in P-5 ve P-22 çeliklerine kıyasla daha üstün olduğu bulunmuştur. Oksitleri incelemek ve TGA sonuçlarını oksit bileşimi ve morfolojisiyle ilişkilendirmek için optik mikroskop, SEM-EDX incelemeleri ve XRD ölçümleri yapılmıştır. P-5 ve P-22 çeliklerinin havadaki daha düşük oksitlenme hızları, yüzeydeki kromca zengin oksit tabakasına dayandırılarak açıklanmıştır. Diğer yandan, $CO_2+2H_2O+7.52N_2$ ortamındaki yüksek oksitlenme hızı, kromun çelik içi oksitlenmesi sonucu oksit tabakasının koruyucu özelliğini kaybetmesiyle açıklanmıştır. Su buharlı ortamların, Cr içeren çelikler için daha korozif olması; yanma reaksiyonu ve/veya su buharının ayrışmasıyla oluşan hidrojenin, kristal kafesi (lattice) içerisine girmesiyle kristal kafesinin genişlemesi ve oksitleyicilere geçirgenliğinin artmasına bağlanmıştır. Su buharı içeren ortamlara serbest oksijen ilavesinin oksitlenme hızını düşürdüğü gösterilmiştir. H_2O'ya O_2 mol oranını gösteren R değerinin, Cr içeren çeliklerin su buharı ortamında serbest oksijen varlığındaki davranışlarının belirlenmesinde önemli bir parametre olduğu bulunmuştur.

To my dear family

ACKNOWLEDGEMENTS

TABLE OF CONTENTS

LIST OF FIGURES

FIGURES

LIST OF TABLES

TABLES

CHAPTER 1

INTRODUCTION

Petroleum is a naturally occurring flammable liquid consisting of a complex mixture of hydrocarbons of various molecular weights and other liquid organic compounds found in rock formations. In an unrefined state it has been utilized by humans for over 5000 years. By the twentieth century, it was in great demand, and had become the most valuable commodity traded on the world markets [1]. The petroleum industry is usually divided into three major components; upstream, midstream and downstream. Upstream sector includes exploration, development and production of crude oil or natural gas. Downstream includes oil tankers, refiners, retailers and consumers. Midstream operations are sometimes classified within the upstream sector, but these operations compose a separate and discrete sector of the petroleum industry. Midstream operations and processes include; gathering, processing/refining, transportation, storage and technological applications.

Oil refinery or petroleum refinery is an industrial process plant where crude oil is processed and refined into more useful products such as; petroleum naphtha, gasoline, diesel fuel, asphalt base, heating oil, kerosene and liquefied petroleum gas [2, 3]. Unprocessed crude oil is not generally useful in industrial applications. However, in the refinery plant, the crude oil is treated to produce different components that can be used as fuels, lubricants, and as feedstock in petrochemical processes. A petroleum refinery consists of many units (heaters, distillation columns, coolers, etc.) work at high temperatures and in corrosive environments. Therefore, in the selection of the construction materials, the corrosion resistance property should be considered along with the mechanical properties. The photographs of furnaces, that are shown in, Figure 1.1 are vertical and horizontal tube type heating furnaces used in petroleum refinery plants [3]. They are designed to raise the feedstock temperature to a proper value before entering the distillation columns in order to increase the efficiency and to reduce the energy consumption. Moreover, corrosion is a factor that can decrease the efficiency of petroleum refinery plant since it causes the failure of equipment items which results in shutting down of the plant totally or partially for maintenance. For example, corrosion problems cost the U.S. petroleum industry about US$3.7 billion per year in 1996 [5, 6].

Figure 1.1 Vertical and horizontal tube type heating furnaces used in petroleum refinery plants [4].

Dry corrosion that is also known as high temperature corrosion plays an important role in the selection of construction materials for refining and petrochemical industries. Oxidation is the most common form of corrosion that faces those industries equipments especially the furnaces. This type of corrosion arises when molecular oxygen (O_2) or other oxidants, such as the air or a combustion atmosphere with or without excess "free" oxygen is present in the environment. In these cases, oxygen activity is controlled by the concentration of molecular oxygen with or without other oxidants. Although alloys achieve their resistance for corrosion by forming protective oxide scales, there is now a growing realization that oxidation may

limit lifetime, either directly through metal wastage or indirectly through raising the local temperatures (and consequently reducing creep-controlled lifetimes) due to the lower thermal conductivity of the oxide scale.

Petroleum refinery heaters (furnaces) are designed to raise the temperature of crude oil to a maximum of about 510°C. The fuel used for heating may be refinery gas, natural gas, residual fuel oils, or combinations, depending on economics, operating conditions, and emission requirements. Figure 1.2 shows schematic cross section of a vertical furnace used at Kırıkkale petroleum refinery plant. The pipes aligned around the walls of the heater are exposed to oxidizing combustion products.
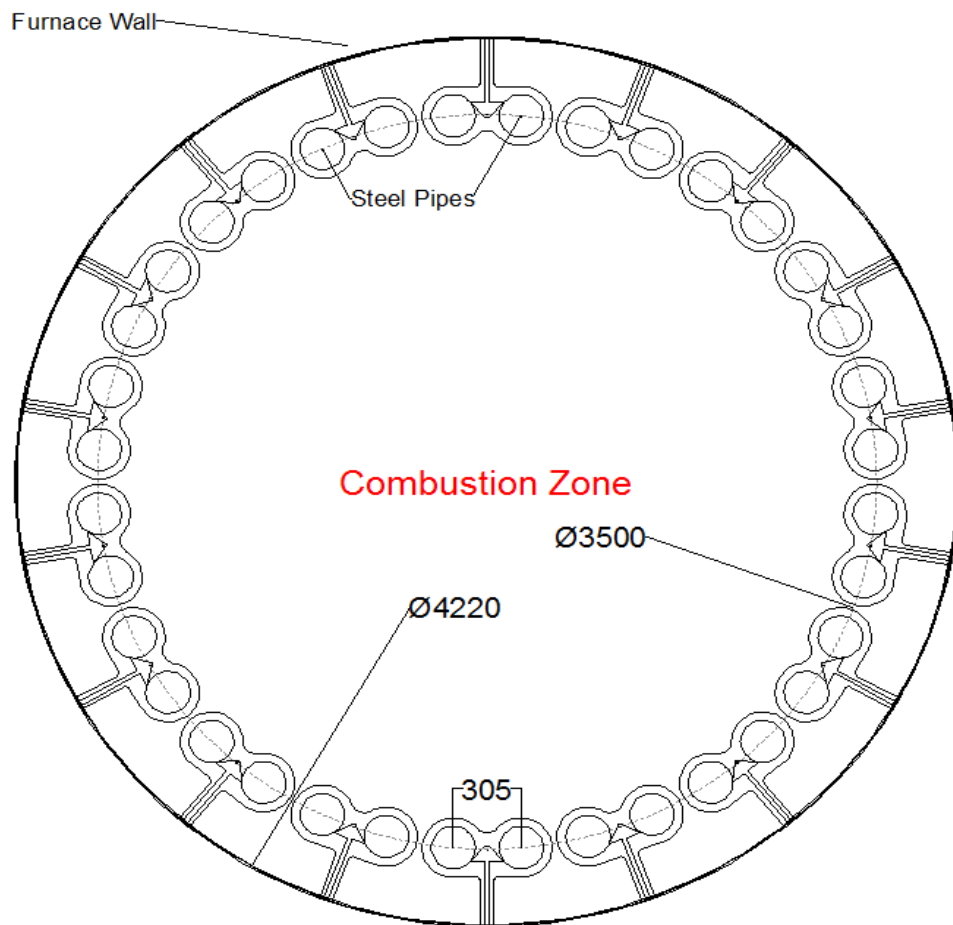
Figure 1.2 Schematic cross section of a vertical furnace used at Kırıkkale petroleum refinery plant

In this study, the first aim was to study the oxidation of four different steels with different chromium contents (C-5, P-11, P-22 and P-5) used in the construction of Kırıkkale petroleum refinery heaters. The oxidation was conducted in two different atmospheres. One of them was dry air and the other was a gas mixture containing $H_2O+N_2+CO_2$ to simulate combustion product of natural gas. The oxidation tests were conducted at two different temperatures (450^oC and 500^oC) by using thermogravimetric analysis technique. Therefore,

the effect of Cr content on oxidation behavior of steels used in petroleum refinery heaters could be studied. The second aim was to determine the conditions for passivation of those steels to reduce the corrosion problems and increase the working life of plant equipment. This was achieved by introducing free oxygen during oxidation in the presence of water vapor. P-91 (9%Cr) steel was used to compare and evaluate the addition of free oxygen during oxidation of P-5(5%Cr) steel in water vapor containing environment. Experiments involved continuous recording of the weight change of the oxidized specimen as a function of time. Further tests such as; X-ray diffraction analysis, optical and scanning electron microscopy (SEM) were done to gain structural, compositional and morphological information on the oxidation products to support the findings of thermogravimetric analysis results.

CHAPTER 2

OXIDATION OF STEELS

Steel is the most commonly used material for construction of many industrial facilities. The selection for different applications depends on satisfying many properties including mechanical and corrosion properties. Different alloying elements such as, C, Cr, Si, Al, Mn, Mo, Ni, etc. are added to the steel to provide the desired properties for the specific application. As a result, operations for long periods without problems that may slow down or in some cases shutdown of the plant could be performed.

2.1 Effect of Alloying Elements on Oxidation of Iron Alloys (steels)

One of the alloying elements is carbon that is very effective on the mechanical properties [7]. From corrosion point of view, the presence of carbon in the steel may result in an increase in oxidation rate since carbon reacts with iron oxide at the scale/base metal interface and evolve CO gas and develop a gap. In high carbon steels at high temperatures, the pressure build up in the gaps cause cracking of the oxide layer formed at the surface and permit the corrosive gases reach the steel surface easily and increase the oxidation rate [8]. Oxidation studies done at $500^{o}C$ [9, 10] showed that the oxidation rate of Fe-C alloy increased when carbon content increased from 0.0 to 1%. On the other hand, at higher temperatures around 600 to $850^{o}C$, the increase of carbon content results in lower oxidation rates than that of pure iron [11, 12]. This lower oxidation rates were explained by the presence of graphite layer between the steel surface and the scale that is capable to reduce the diffusion of iron and/or oxygen ions and hence reduces the oxidation rate [11].

Silicon is a less noble element compared to iron, so the formation of silicon-rich layer on steel surface decreases the oxidation rates of Fe-Si alloys. The slower oxidation rate was probably due to the lower diffusion rate of silicon through the oxide layers and the hindered iron ion diffusion through the SiO_2 layer. Addition of small amounts of silicon were found to reduce the oxidation rate of Fe–Cr model alloys by improving the ability to develop protective chromia scales during oxidation in H_2O containing environments [13]. Huntz et al. [14] showed that addition of Si up to 4% to steel similar to P-91 which contains 0.45% Si, form oxides of both Fe and Cr when oxidized in argon containing trace amounts of H_2 and H_2O, stabilized the formation of protective continuous chromia layer. They attributed these results to the formation of a silica layer that lowered the local P_{O2} on the surface so that Fe-oxides became unstable. Moreover, they proposed that Cr can diffuse through the silica to form the chromia scale but Fe was blocked by the silica.

Similar to Si, Al forms an aluminum-rich layer at the scale/base metal interface that hinders iron ion diffusion and reduces the oxidation rate. The morphology of formed aluminum oxide depends on; aluminum content of the steel, the temperature, and the oxidizing

atmosphere. Saequsa et al. [15] found that in 500-700°C temperature range Al_2O_3 is the stable aluminum-rich layer during oxidation of Fe-1wt % Al alloy in 1 atm O_2, whereas, in 700-900°C temperature range such layer was $FeAl_2O_4$ spinel in the same environment.

Additionally, manganese is also added to steels to improve oxidation resistance, but its effect was sometimes negative. Zurek et al. [16] noticed that opposite to Si that significantly reduces the oxidation rate of Cr steels, Mn seems to increase it since Mn forms a spinel oxide of $MnO \cdot Cr_2O_3$ rather than the protective chromia oxide.

Molybdenum is more noble than iron. Addition of about 0.013% Mo to silicon steels results in good oxidation resistance since molybdenum concentration increases near the surface [17]. Lepingle et al. [18] reported that T22 and T91 steels have 1%Mo had lower corrosion rate during oxidation in pure steam at 650°C compared to those of T23 and T92 containing much lower concentrations of Mo. In contrast, Schutze et al. recommend that molybdenum content should be at the lowest levels for the steels to be used in the presence of water vapour [19].

Nickel is more noble than iron and it has also been shown to enhance the oxidation resistance by reducing the cation diffusion in the Cr_2O_3 scale and preventing the formation of $FeCr_2O_4$ and Fe_2O_3. Consequently, the iron matrix of nickel steel is selectively oxidized and nickel is rejected at the oxide/base metal interface [20]. This thin, Ni concentrated layer results in interpenetration of the oxide and metal at the interface and produces a tight mechanical oxide-metal bond and substantially increases the oxidation resistance.

2.2 Behavior of Chromium during Oxidation of steels

The high value of chromium metal is due to its high corrosion resistance and it can be added to steels to form Fe-Cr alloys. There are approximately 4.4 million metric tons of marketable chromite ore, and about 3.3 million tons of Fe-Cr alloys with an approximate market value of 2.5 billion United States dollars were produced in 2000 [21]. These Fe-Cr alloys are widely used in the construction of many high temperature industrial equipments. Depending on chromium content, gas composition, and temperature, Fe-Cr steels may form a protective Cr rich oxide or non-protective iron rich oxide layers on the surface.

2.2.1 Oxidation of Chromium in the Air

Chromium in its pure state or in Fe-Cr alloys oxidizes when exposed to oxygen or air even at room temperature and the result is the formation of protective solid scale on the metal surfaces. As seen in Figure 2.1, chromium (III) oxide (Cr_2O_3) is the most stable oxide over a wide temperature range. Formation of Cr_2O_3 on the steel surface provides the protection against oxidation and makes Fe-Cr alloys satisfy the requirements to be used in high temperature applications.
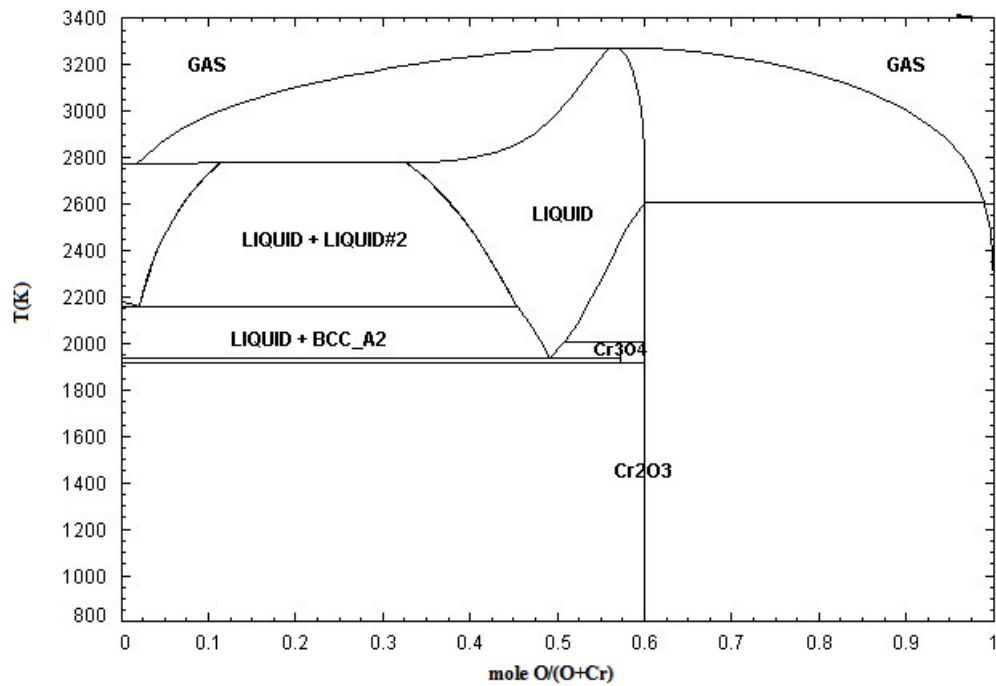
Figure 2.1 Chromium oxygen phase diagram[22]

2.2.2 Oxidation of Chromium in the Presence of Water Vapor

The presence of water vapor in the oxidizing environment leads to a higher oxidation rate of Fe-Cr alloys than air oxidation. This was noticed by many researchers and they concluded that the behavior of Cr in dry and wet environments is completely different. In dry air oxidation, Cr forms a protective oxide layer on the steel surface that is able to protect the steel from oxidation and make the corrosion rate slow. But in wet oxidation the protective effect of Cr is somehow lost and the oxide formed is non-protective iron oxides resulting in high corrosion rate.

2.2.3 Oxidation Mechanisms of Cr in H$_2$O-containing Gases

A lot of work [23-40] was conducted to explain the relation between the high corrosion rate and water vapour during high temperature oxidation of Cr, Fe–Cr and Fe–Cr–Ni alloys. The high corrosion rate was attributed to the higher corrosivity of water vapor and the loss of the protective effect of chromium.

2.2.3.1 Higher Corrosivity of Water Vapor

The higher corrosivity of water could be the result of:

Water vapor dissociates on the steel surface according to the reaction (2.1) and provides hydrogen and oxygen to the scale which result in increase in the corrosion rate.

$$H_2O \rightarrow H_2 + \frac{1}{2} O_2 \tag{2.1}$$
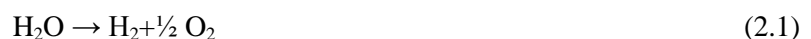
In the presence of water vapor, the increase in cation diffusion rate leads to condensation of vacancies in the scale and the result is a porous scale formation [39]. The resulted hydrogen from eq.(2.1) may accumulate inside these pores and create pressure that build up and cause scale cracking. These cracks act like channels for the oxidant gases to penetrate easier and expedite the oxidation.

2.2.3.2 Losses of Protective Effect of Chromium

2.2.3.2.1 Formation and Volatilization of $CrO_2(OH)_2$

The formation of volatile Cr species, such as $CrO_3(g)$, or $CrO_2(OH)_2(g)$ [25, 41, 42] at high temperatures according to the chemical reactions given below, leads to a depletion of Cr in the scale and an increase in the corrosion rate.

$$\frac{1}{2} Cr_2O_3(s) + \frac{3}{4} O_2(g) = CrO_3(g) \tag{2.2}$$

$$\frac{1}{2} Cr_2O_3(s) + \frac{3}{4} O_2(g) + H_2O(g) = CrO_2(OH)_2(g) \tag{2.3}$$

The thermodynamic data for $CrO_2(OH)_2$ has confirmed that it is more stable than all other volatile chromium species at temperatures below 1000^oC [43]. In wet air, when there is high water vapor and oxygen partial pressures, the formation of volatile $CrO_2(OH)_2$ leads to formation of Fe-rich oxide layers on the steel surface and losses of protection against the oxidation [45-48]. Asteman et al. [31, 32] found that during oxidation of 304L (Fe–18Cr–8Ni) stainless steel at 600^oC in O_2–H_2O gas mixtures, the large weight gain when P_{H2O} was increased was due to lower Cr/Fe ratio in the scale as a result of Cr evaporation.

The study of Caplan and Cohen [46] showed that presence of water with oxygen resulted in higher weight loss from Cr_2O_3 formed on the surface due to increase in evaporation rate. Furthermore, similar behavior was seen by Hänsel [48] since he found that adding water vapour to the air increases the evaporation rates.

2.2.3.2.2 Internal Oxidation

The internal oxidation occurs when atomic oxygen dissolves into an alloy at the external oxide-metal interface and it diffuses into the metal matrix to oxidize a more reactive alloying element rather than the solvent metal. The oxidation results of Fe-Cr alloys in water vapor containing environments showed the formation of Fe-rich oxide layers on the steel surface and a zone with internal precipitates of Cr-rich oxide beneath the surface [25, 49]. According to studies done [50-52], the effect of water vapor was attributed to the presence of hydrogen since it was found that the presence of water vapor on one side has an effect on the oxidation behavior of the other side exposed to the air and the reason for this was the diffusion of hydrogen which was available from the dissociation of water through the steel. Setiawan et al. [53] suggested that hydrogen provided from water dissociation dissolved in the internal oxidation zone (IOZ) and segregated at the oxide-metal matrix interface led to an increase in the inward oxygen flow to the steel then caused internal oxidation of the chromium and the result was higher corrosion rate. They found that the permeability of oxygen into steel was higher by a factor of 1.4 in wet environment than the air and the Cr% for transition from internal to external oxidation is higher by a factor of 1.2. The results of pure iron and ternary Fe-Cr-C alloy oxidation done by M.Nakai et.al.[54] showed that hydrogen dissolved more in

ternary steel than pure iron since hydrogen preferentially dissolves in $(Fe,Cr)_3O_4$ oxide layer which leads to a higher corrosion rate in wet environments. Stott at al. [55] proposed that the oxygen transport in (IOZ) takes place along the interface between oxide particle and metal matrix and through the internal oxide precipitate in the alloy. So it could be summarized that the presence of water vapor in the oxidizing gases provides hydrogen that can dissolve in the alloy and ease the delivery of oxidant gas inside the steel making chromium oxidize internally, and it results in higher oxidation rate than in dry gases [34].

2.2.4 Oxidation in the presence of carbon dioxide

The martensitic 9 wt% Cr steels, such as P-91 or P-92, were able to form protective oxide layers in air within the temperature range of 550-600°C. On the other hand, 20 wt% chromium content was required to get a similar protection when these steels oxidize in environment rich in CO_2 [37]. According to Giggins et al. [56] while Fe-35%Cr steel was able to form a continuous Cr_2O_3 layer on the surface, Fe-15Cr was not and the corrosion rate was higher during oxidation in pure CO_2 at 900°C. Their results were in agreement with Fujii and Meussner [57] and they explained this behavior by the formation of internal carbides in the case of Fe–15Cr. The corrosivity of CO_2 can be explained as, CO_2 dissociate to provide oxygen via the reaction:

$$CO_2(g) \rightarrow CO(g) + \frac{1}{2}O_2(g) \tag{2.4}$$

The increase in the CO/CO$_2$ ratio increases the local activity of carbon through the equilibrium:

$$2CO(g) \rightarrow CO_2(g) + C(s) \tag{2.5}$$

Then carbon reacts with Cr forming chromium carbides and the result is a shortage of Cr that is needed to form a protective Cr_2O_3 layer. Gerald et al. [13] studied the oxidation of different ferritic martensitic Fe–Cr base alloys in the air, Ar-30%CO$_2$ and Ar-50%CO$_2$ gas mixtures at 500-650°C temperature range. And they found that the presence of CO$_2$ caused a higher corrosion rate despite the lower oxygen partial pressure compared to the air. They related the higher corrosivity of CO$_2$ containing environment to carbide formation that was responsible for chromium depletion near the metal oxide interface and loss of the protective effect of chromium.

2.3 Thermodynamics

Chromium is very reactive and it reacts with oxygen in oxidizing environments and forms chromium oxide according to the following reaction:

$$2Cr + + \frac{1}{2}O_2 \rightarrow Cr_2O_3 \tag{2.6}$$

From thermodynamic point of view, the criteria for oxide formation, is the negative Gibbs energy change (ΔG) for the above reaction to take place in the written direction. Thermodynamically, an oxide is likely to form on a metal surface when the oxygen potential in the environment is greater than the equilibrium oxygen partial pressure. The equilibrium

oxygen partial pressure can be determined from the standard Gibbs energy of formation of the oxide as:

$$\Delta G^o = -R.T.\ln\left(\frac{a_{Cr_2O_3}}{a_{Cr}^2 \cdot P_{O_2}^{3/2}}\right)$$

(2.7)

When the activities of the solids; such as, metal and the oxide are unity, eq. (2.7) becomes:

$$\Delta G^o = R.T.\ln P_{O_2}^{3/2}$$

(2.8)

Then, this yields partial pressure of oxygen in equilibrium with pure metal and oxide as:

$$P_{O_2} = e^{\left(2\Delta G^o/3RT\right)}$$

(2.9)

When the metal is working in environment that contains a mixture of combustion product gases like CO_2, N_2, H_2O without molecular oxygen, the oxygen potential is controlled by P_{H_2}/P_{H_2O} and/or P_{CO}/P_{CO_2}. Besides, the oxygen potential can be determined by the reaction:

$$2H_2 + O_2 \Leftrightarrow 2H_2O$$

(1.10)

The standard Gibbs energy of formation is related to the partial pressures of hydrogen, oxygen, and water vapor as:

$$\Delta G^o = -R.T.\ln\left(\frac{P_{H_2O}^2}{P_{H_2}^2.P_{O_2}}\right)$$

(2.11)

Rearranging the eq.10 results in:

$$P_{O_2} = \frac{e^{\left(\Delta G^o/RT\right)}}{\left(P_{H_2}/P_{H_2O}\right)^2}$$

(2.12)

Thus, the equilibrium oxygen partial pressures at various temperatures can be determined as a function of P_{H_2}/P_{H_2O}.

The equilibrium reaction for an environment whose oxygen potential is controlled by P_{CO}/P_{CO_2} is:

$$2CO + O_2 \Leftrightarrow 2CO_2$$

(2.13)

The corresponding oxygen potential is:

$$p_{O_2} = \frac{e^{\left(\Delta G^o / RT\right)}}{\left(P_{CO}/P_{CO_2}\right)^2}$$

<div align="right">(2.14)</div>

Ellingham/Richardson diagram given in Figure 2.2 shows the equilibrium pressure values for different metal oxide systems at different temperatures. When oxygen partial pressure in the environment is equal to the equilibrium value, there will not be a driving force for the reaction to take place and both metal and oxide are stable. At oxygen partial pressures higher than the equilibrium value, oxide formation will be spontaneous, whereas at lower values dissociation of the oxide will be spontaneous. Hence, values of equilibrium oxygen partial pressures corresponding to standard Gibbs energy of formation of the oxide for different elements can be obtained from Figure 2.2. In the case of elements that have several oxides like iron, equilibrium oxygen partial pressures increase as the oxygen content of the oxide increase. The reverse is true during dissociation for example, iron oxides dissociate according to: Fe_2O_3 to Fe_3O_4, Fe_3O_4 to FeO and FeO to Fe as oxygen partial pressure decrease.

2.4 Oxidation Kinetics

Thermodynamic calculations can only show us whether the reaction between metal and oxygen is possible or not. But, kinetics gives us how reaction is taking place and how fast it is taking place (reaction rate). In order to determine the rate of a reaction, the mechanism of the process is important. The mechanism of metal oxidation at elevated temperatures can be thought as series of stepwise processes broken down as follows:

1- Chemisorption of a gaseous component.

2- Dissociation and electron transfer by the gaseous molecule.

3- Nucleation and crystal growth.

4- Diffusion and transport of cations, anions, and electrons through the scale.

The most important parameter of metal oxidation from an engineering viewpoint is the reaction rate. The reaction rate is controlled by the slowest step from the four steps given above. Many factors such as temperature, oxygen partial pressure, elapsed time of reaction, surface preparation, and pretreatment of the metal affect the oxidation reaction rate.
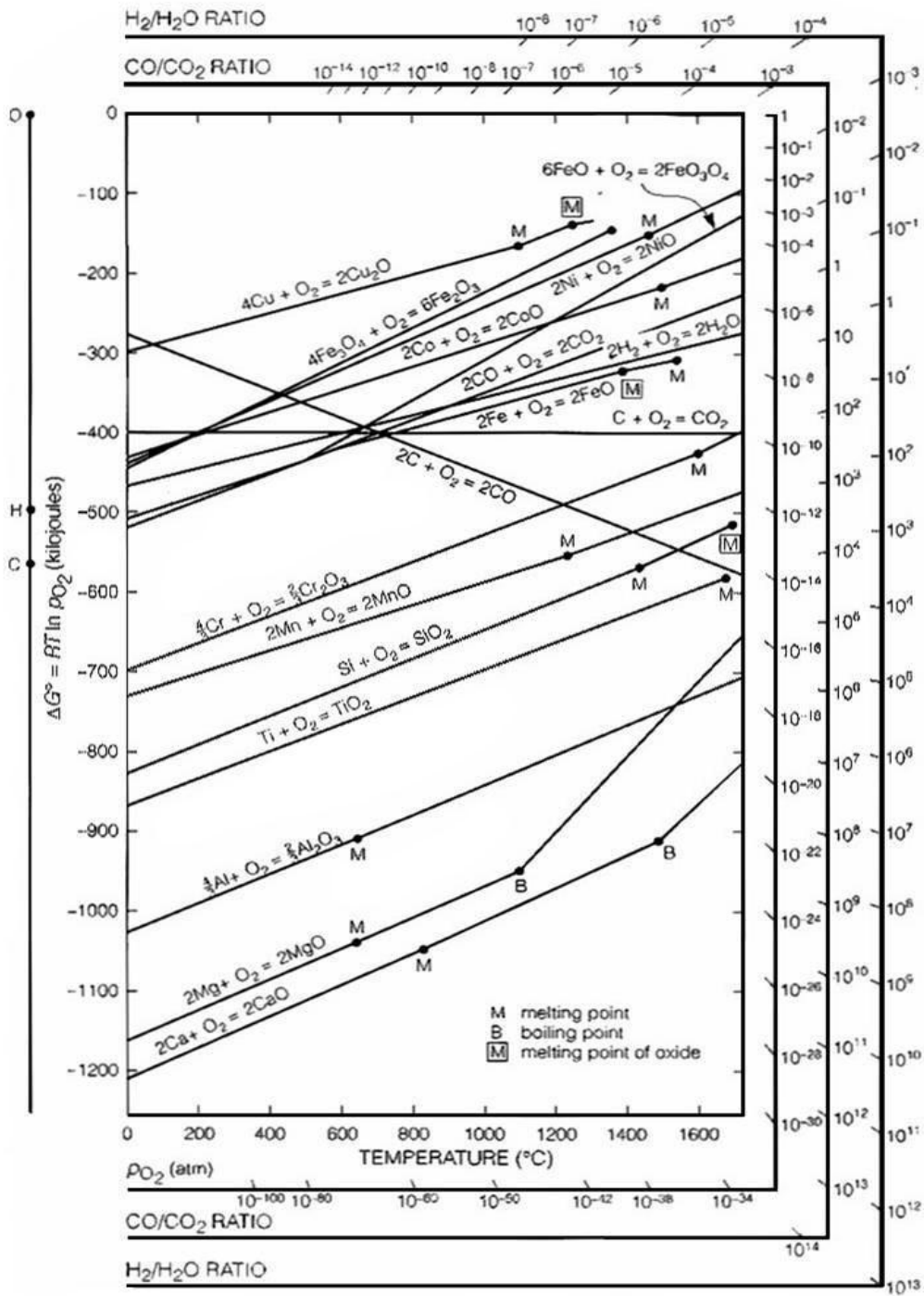
Figure 2.2 Ellingham diagram for metal oxide compounds [58]

Oxidation reactions result in solid products retained on the metal surface, so the rate of oxidation is usually measured and expressed as weight change per unit area. Empirical rate laws sometimes observed during oxidation of various metals under different conditions are illustrated in Figure 2.3. They usually are given as a plot of weight gain per unit area versus time. The simplest empirical relationship is the linear law,

$$W = k_t.t$$

(2.15)

Where W is weight gain per unit area, t is time, and k_t is the linear rate constant. Linear oxidation is characteristic of metals that form a porous or cracked scale. Therefore, the scale does not represent a diffusion barrier between the two reactants.

In 1933, C. Wagner showed that the ideal ionic diffusion-controlled oxidation of pure metals should follow a parabolic oxidation rate law [59]. Therefore, the decrease in oxidation rate with time during oxidation of pure metals could be explained with reference to increase in diffusion path with time. The empirical equation for the parabolic law is,

$$W^2 = k_p.t + c$$

(2.16)

Where k_p is the parabolic rate constant and c is a constant. The form of the parabolic oxidation equation is typical of non-steady-state diffusion-controlled reactions. The logarithmic empirical reaction rate law,

$$W = k_e.\log(c.t + A)$$

(2.17)

Where: k_e, c, and A are constants. Logarithmic oxidation behavior is generally observed when thin oxide layers (e.g., less than 100 nm) are formed at low temperatures.
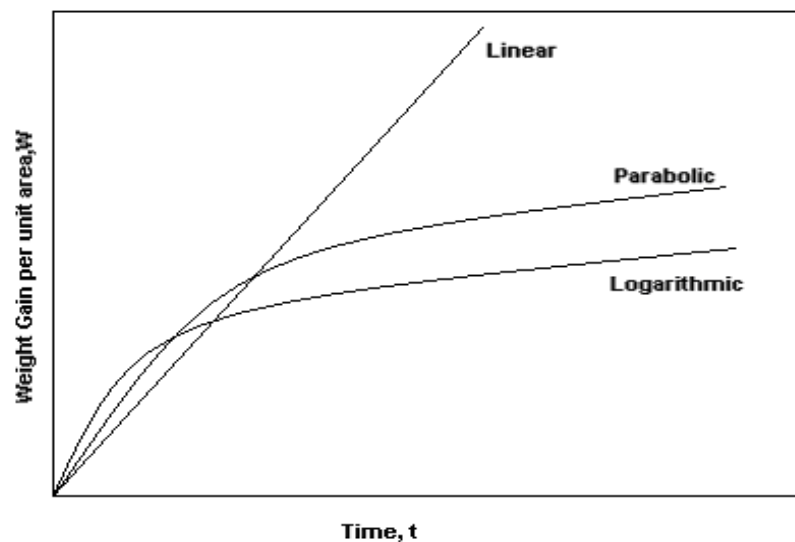
Figure 2.3 Oxidation film growth curves for linear, parabolic, and logarithmic rate equations [59]

In some cases, shifting from parabolic to linear oxidation is taking place. This can be seen when a compact scale growing at a parabolic rate transforms to an outer porous and non-protective oxide layer. This combination between parabolic and linear oxidation called paralinear oxidation [60]. After long periods, the oxidation becomes essentially linear and the concurrently inner layer approaches a stationary thickness; that is, it grows at the same rate at which it is consumed by the linear depletion.

2.5 Experimental Measurements of High Temperature Oxidation of Metals

Laboratory tests are often conducted under accelerated conditions (e.g., higher temperatures and/or more corrosive environments) in order to increase the confidence level and produce results in a short period of time. The accelerated test is also frequently used for initial alloy screening to narrow down the viable candidates for long term tests and/or field trials. Extreme care should be taken if the results of short-term tests and/or accelerated tests are going to be used for life time assessments. The gravimetric method is widely used to study oxidation and/or other forms of high temperature reactions. This test method involves measurements of mass change of sample with temperature and time by using a thermobalance.

A thermobalance is a combination of a suitable electronic microbalance with; furnace, temperature controller and a computer (Figure 2.4). Thermogravimetric Analysis is a technique that monitors changes in the mass of usually a solid sample as a function of time and temperature. Continuous recording of the change in weight of a sample makes the gravimetric method widely used in the high temperature oxidation studies. But the availability of testing just one sample in each run makes it unsuitable for generating an engineering database for many different alloys since it is a lengthy process [61].
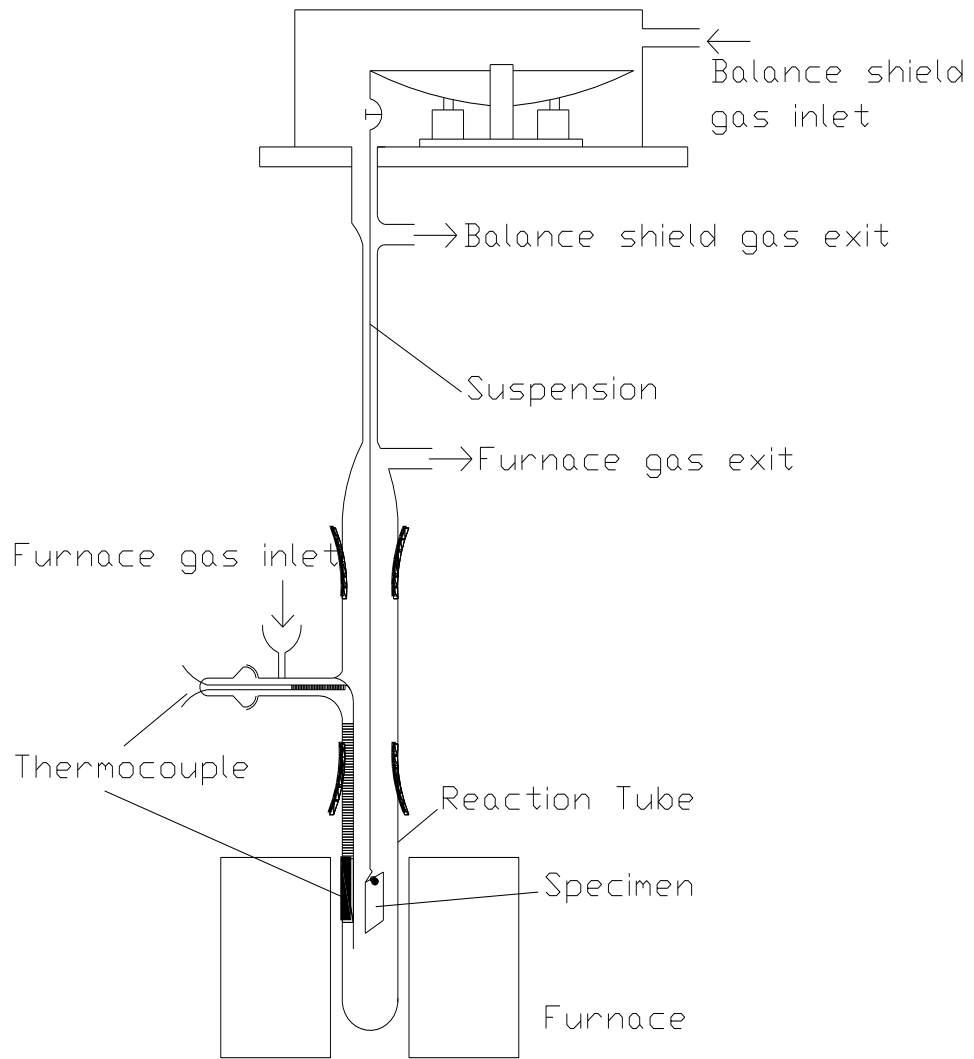
Figure 2.4 Schematic figure of electrobalance for use in oxidation tests [61]

CHAPTER 3

EXPERIMENTAL PROCEDURE

3.1 Introduction

The thermogravimetric technique employing an electrobalance was used to study high temperature corrosion of steels used in the construction of petroleum refinery heaters in this research. The experiments involved continuous measurements of weight changes of the samples under controlled atmospheres at 450 and 500°C. The analyses of the oxidation products were carried out by using X-ray, optical and scanning electron microscopes to correlate the weight gain data to the nature of the products obtained from oxidation.

3.2 Materials

In this research work, four different steels (C-5, P-11, P-22 and P-5) with different chemical compositions (wt %), given in Table 3.1, were used in the oxidation experiments. The chemical composition of P-91steel was added to Table 3.1 because this steel was used to compare the behavior of P-5 in moist atmosphere containing free oxygen. The steels, delivered by Kırıkkale Petroleum Refinery Plant in tubular form, were used in the construction of petroleum refinery heaters. The original diameters of the tubes are given in millimeters under Φ column of Table 3.1. In order to prepare test specimens, they were cut and machined into flat and thin steel pieces. The steel specimens were subjected to heat treatment involved heating up to 700 ^{o}C, keeping there for 1 hr and cooling them inside the furnace. The microstructure of the steels were examined under optical microscope and the results are given in Figure 3.1. From this figure it can be seen that the microstructure of all steels were similar therefore, the grain size effect on the oxidation behavior of these steels could be ignored.

Table 3.1 Chemical compositions of the steels

Steel	ASTM	Φ(mm)	%C	%Mn	%P	%S	%Si	%Cr	%Mo	%V
C-5	A 106	152	0.25	0.65	0.047	0.055	0.11	--	--	--
P-11	A 335	152	0.15	0.45	0.03	0.03	0.77	1.25	0.57	--
P-22	A 335	108	0.15	0.47	0.03	0.03	0.45	2.25	1.0	--
P-5	A335	152	0.14	0.45	0.03	0.03	0.45	5.0	0.55	--
P-91	A335	--	0.09	0.5	--	--	0.4	9.2	0.9	0.22
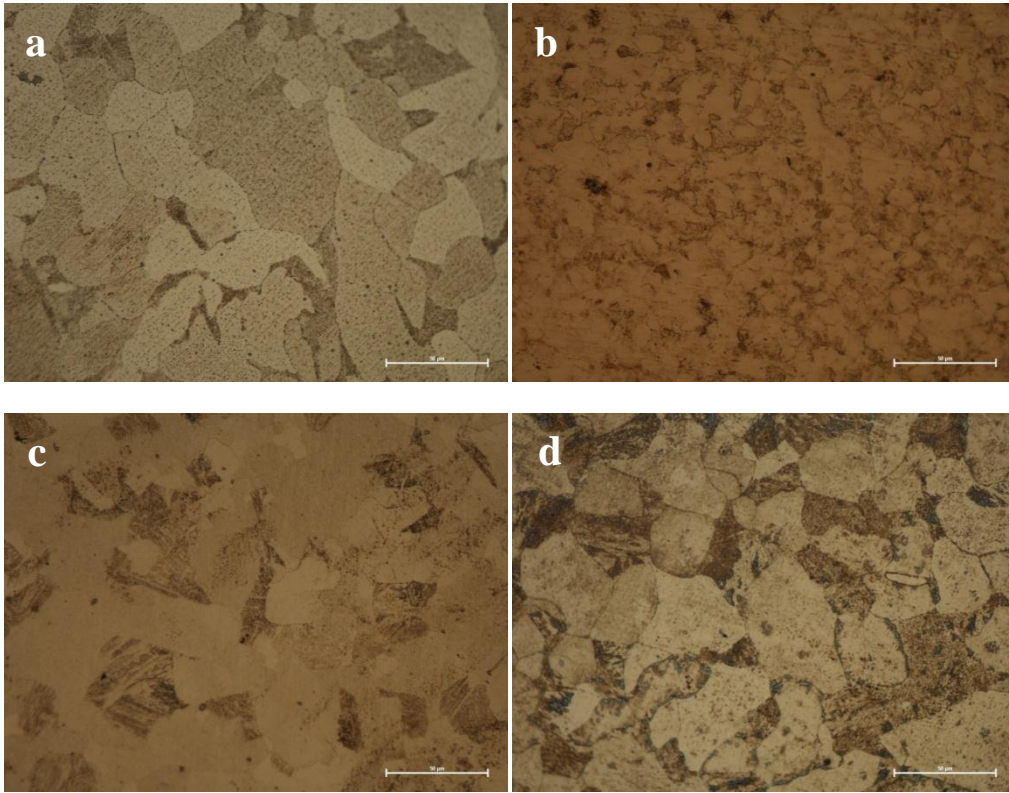
Figure 3.1 Optical photographs of internal structure of a) C-5, b) P-5, c) P-11 and d) P-22 (500X)

3.3 Preparation of Samples

The steels samples were divided into two sets as shown in Figure 3.1. The first set (a) had dimensions of 50 mm x 25 mm x 2 mm and was used to provide accurate experimental data by oxidizing a large area during the experiments. The other set (b) with dimensions of 10 mm x 10 mm x 2 mm subjected to oxidation together with the large samples were used to prepare samples (c) for further tests such as; microscopic, X-ray and SEM analysis. The large samples were prepared with two holes having 3 mm diameter at its two ends. One of these holes was used to suspend the large sample to the electrobalance while the other to suspend the small sample that also had a hole of 3 mm diameter. Both samples were suspended with quartz hooks. The effects of sharp corners and edges were prevented by rounding them.
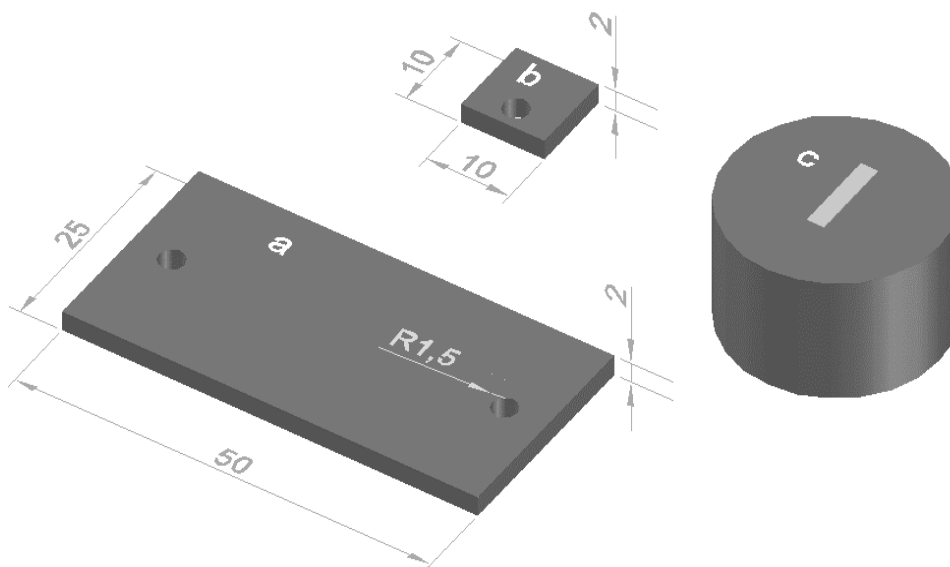
Figure 3.2 Schematic diagrams of (a) sample that has large area, (b) sample to prepare specimens and (c) mounted sample to examine the cross section of sample (b)

Using SiC papers, the steel samples were ground sequentially by starting from 120 grit and following 220, 320, 400 and 600 grits. The samples were ultrasonically cleaned and degreased by using alcohol to remove SiC and the steel particles left from the grinding. In high temperature corrosion studies, grinding without polishing was recommended to provide a surface that favored the nucleation of oxides and result in dense adherent scales. The surface areas of samples were calculated after measuring the dimensions of both samples with the aid of a micrometer.

3.4 Thermogravimetric Analysis (TGA)

A CAHN C-1000 electrobalance was used for the thermogravimetric analysis in this study (see Figure 3.3). The balance consisted of two parts; weighing and controlling units. The sample weight change during oxidation was detected by the weighing unit, while this weight change was converted to an electrical signals (voltage) output by the controlling unit. These output signals were read and converted to weight change on a digital computer through a data acquisition unit. At the beginning of each experiment, the weight was zeroed by mechanical and electronic taring using those two units. The steel samples were hanged to the weighing unit by a quartz hook in the middle of a Pyrex reaction tube in the hot zone of the furnace. The reaction tube had a diameter and a length of 5 and 80 cm respectively and it was extended out of a vertical split furnace from both ends. The upper end of the reaction tube was connected the bottom of the weighing unit and the lower end was left open to the atmosphere.
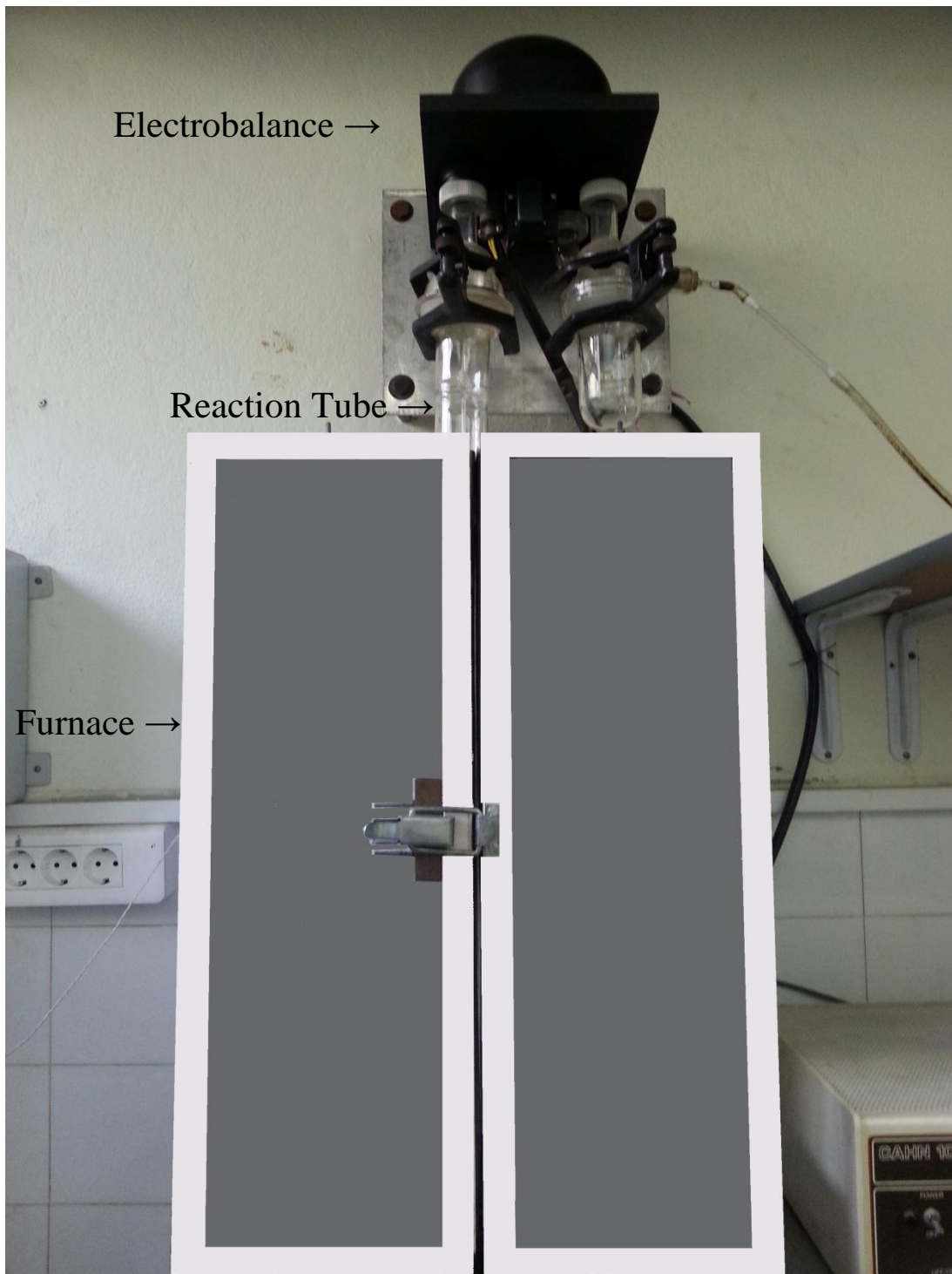
Figure 3.3 Photo of the electrobalance used in oxidation tests

Schematic representation of the experimental setup is given in Figure 3.4. From the auxiliary apparatus it can be seen that this set-up was used in experiments where the gas phase contained water vapor carbon dioxide and nitrogen.
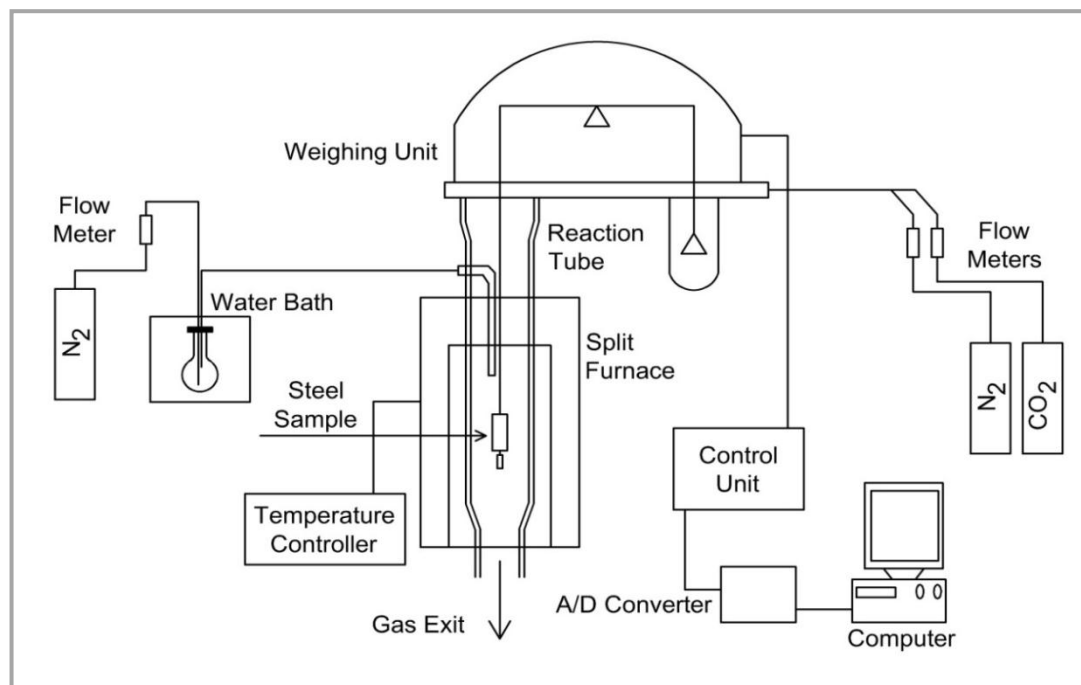
Figure 3.4 Schematic representation of setup for oxidation tests using $CO_2+H_2O +N_2$ mixture

LINDBERG LHTF322C split type cylindrical furnace was used vertically to provide the heat necessary for high temperature oxidation tests. And the furnace was connected to a Eurotherm temperature controller that was adjusted to set the desired temperature ($\pm1^{o}$C) for the oxidation reaction.

The oxidation tests of four different steels were done in air and in $CO_2+H_2O+N_2$ mixture at 450°C and 500°C. The durations changing between 35 to 96 hours were used. It was found that the nature of the oxides did not change for long and short oxidation periods, and 48 hours of oxidation period was selected for most of the tests in this study. During the oxidation tests, the total flow rate of the oxidizing gases was controlled at room temperature to be 895 cc/min for 450°C and 837 cc/min for 500°C. These flow rates are equivalent to 120 cm/min gas velocity in the reaction chamber. In air oxidation experiments, the above flow rates were delivered into the reaction chamber through the upper part by means of an air pump.

The experiments involving $CO_2+H_2O+N_2$ mixture, to simulate combustion product of natural gas, were conducted by using CO_2 and N_2 gas cylinders (with technical grade) instead of the air pump. The amount of each gas was measured by flow meters to prepare the desired gas composition. Part of the N_2 gas was passed through water in a constant temperature bath to provide the desired water vapor concentration in the gas phase. The bath temperature was experimentally determined to be 61°C and 60°C respectively for 450°C and 500°C tests to get

the desired water vapor partial pressure for the TGA tests. To minimize the upward movement of the H_2O+N_2 mixture, H_2O+N_2 mixture was delivered into the reaction tube directly from entrance port at the left hand side of the tube while the remaining gases were sent from the upper part. In order to eliminate the condensation of water vapor outside the reaction tube, the glass piping carrying the H_2O+N_2 mixture was covered by a heating tape. Given in Table 3.2 are the distribution and flow rates of the gases used in the oxidation by $CO_2 +H_2O+N_2$ gas mixture at 450°C and 500°C.

Table 3.2 The distribution of gas flow rates used in $CO_2+N_2+H_2O$ environment at 450°C and 500°C

Flow rate (cm^3/min)	N$_2$			CO$_2$			H$_2$O		
	U.P	S.P	T	U.P	S.P	T	U.P	S.P	T
450°C	136.2	570.8	707	62.7	-	62.7	-	125.2	125.2
500°C	127.4	533.9	661.3	58.6	-	58.6	-	117.2	117.2

U.P: upper port, S.P: side port, T: total

To provide an inert atmosphere and to assure that the sample was not oxidized during heating, the reaction tube and the balance were flushed by a flow of nitrogen gas. After the reaction temperature was reached and before the commencement of the experiment, sufficient volume of reaction gases was supplied through the reaction chamber for about 5 minutes to quickly fill the apparatus with the desired gas composition and this was used to eliminate the small weight change of the sample due to density differences of the gases. Thereafter, the flow rates of the gases were maintained at the above levels in the course of each experiment.

Furthermore, the weight changes of the samples subjected to oxidation were recorded by using a PCLD 711 analog-to-digital (A/D) converter via a computer system. In this study, a 100 milligram recording range (with an accuracy of 0.1% of recording range) was used for 48 hours oxidation experiments with overall accuracy of ±0.2 mg. A BASIC computer code was used to program the computer to get a reading from the data acquisition unit for every minute. After each experiment, the supply of the oxidizing gases was cut, but the continuous flow of the N_2 gas was maintained through the reaction tube until the system was cooled down. After cooling the furnace, the samples were taken out from the furnace and kept in desiccators for subsequent analysis of the oxidation products.

In addition to the oxidation experiments mentioned above, other tests were conducted to examine the effect of oxygen in water vapor containing environments. It was expected that introduction of free oxygen along with water vapor could reduce the oxidation rate by forming protective chromium containing oxide and possibly passivate the surface of those steels. P-5 steel was subjected to oxidation to study the effect of inserting free oxygen. The gas phase composition changing from air (21% O_2 + 79% N_2) to 21% H_2O + 79% N_2 was used to cover a range of composition determined by an experimental design procedure. The gas phase compositions are given in Table 3.3 and they are presented on an A-B-C

composition triangle in Figure 3.5. The minimum number of experiments needed to cover the entire composition triangle was calculated by using a minimal factor program. The fractions given in Table 3.3 corresponds to fractions of A (21% H_2O + 79% air), B (air; 21% O_2 + 79% N_2) and C (21% H_2O + 79% N_2).

Table 3.3 Minimal factor program calculation results for fractions of A, B and C gas compositions

point→ com.↓	1	2	3	4	5	6	7	8	9	10
A (H_2O+air)	0	0.5	0.333	0.1667	0	0.6667	0.1667	1	0.5	0
B (air)	0	0.5	0.333	0.6667	1	0.1667	0.1667	0	0	0.5
C (H_2O+N_2)	1	0	0.333	0.1667	0	0.1667	0.6667	0	0.5	0.5

A
0.21H₂O+0.79Air

8

6

2   9

3

4   7

5   10   1

0.21O₂+0.79N₂   0.21H₂O+0.79N₂
B   **C**
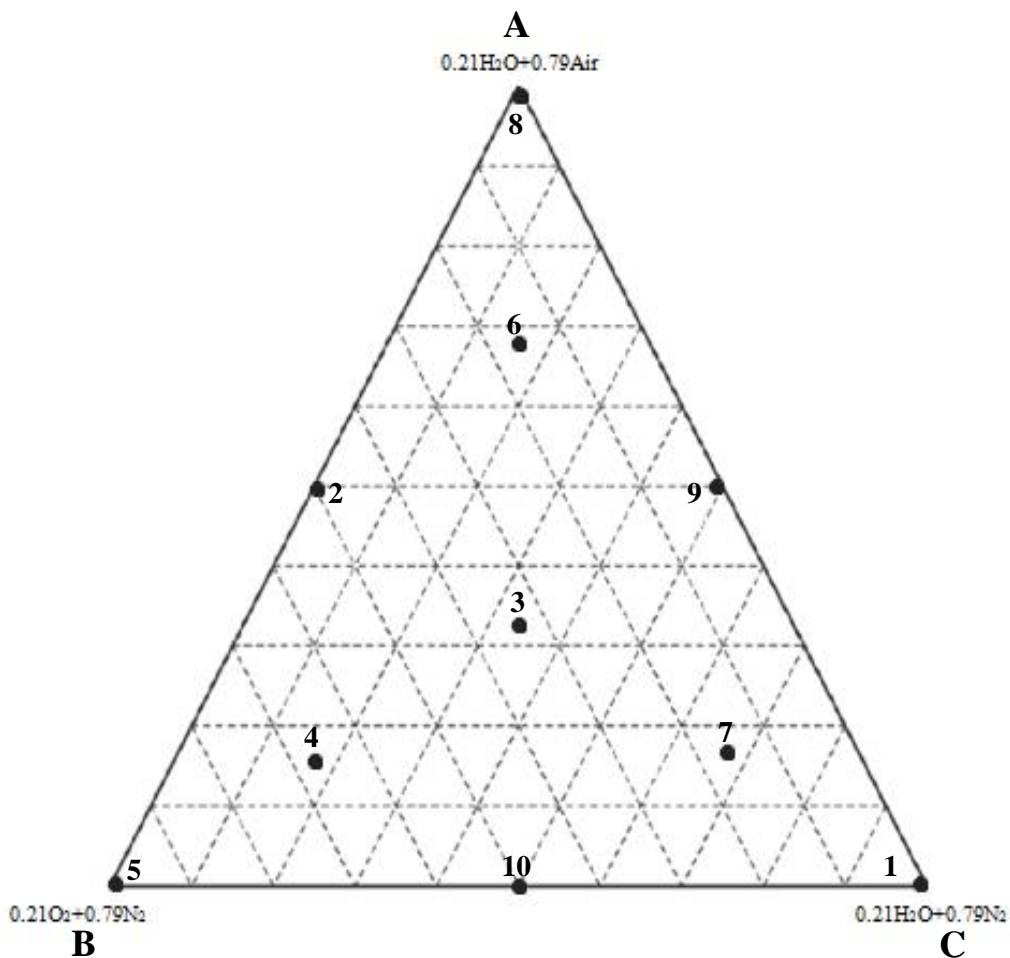
Figure 3.5 Distribution of the points on the composition triangle

The weight gain data during oxidation of P-91 (9%Cr) steel in 21% H_2O + 79% % N_2 was used to compare and evaluate the effect of free oxygen addition during oxidation of P-5 (5%Cr) steel in water vapor containing environments.

In addition, effect of charging of P-5 steel with hydrogen was studied by keeping steel sample in a 40%H_2-60%Ar gas mixture for 4 hours at 500°C prior to subjecting the sample to oxidation in air. This test was performed to observe the effect of hydrogen introduction to the structure and the behavior of Cr during oxidation after charging the steel with hydrogen.

3.5 Identification of Oxidation Products

The phase identification and structural investigation of the products obtained from the oxidation were carried out by the aid of X-ray diffractions, optical and electron microscope. The 10 mm x 10 mm x 2 mm specimens were mounted in bakelite (see Figure 3.1(c)) for above purpose. The mounting was done so as to have the cross section of the oxide film perpendicular to the specimen surface. Then, they were ground, polished and investigated

under OLYMPUS optical microscope. Also, the same samples were examined by scanning electron microscope (JEOL JSM 6400).

Rigaku D/MAX2200/PC machine with Cu K_α target, λ= 0.154056 nm was used for X-ray diffraction (XRD) study of the oxidized samples. Since the depth of the oxide scales were very small to be removed mechanically and ground to powder, the small specimens themselves were used for the XRD analysis by placing the largest surface against the diffraction beam. The quantitative X-ray diffraction analyses were not considered because the relative intensities of the oxide phases might not represent the true relative intensities since the oxide scales formed on the metal surface might have preferred orientation of the metal grains. Besides, the diffractions from the metal under the oxide films might interfere with the intensities of the diffractions coming from the oxide layers.

CHAPTER 4

RESULTS

4.1 Introduction

The thermogravimetric test results of the four steels are shown in the figures below (Figures. 4.1, 4.2, 4.4 and 4.5). These figures are representing the change in weight gain (mg/cm^2) with time (hr) at 450°C and 500°C in two different oxidizing atmospheres over a period of 48 hours. The resulted graphs clearly show that all the steels oxidized in this study follow the parabolic form under both oxidation conditions.

4.2 Oxidation in Air

In air oxidation, the weight gain vs. time graphs given in Figures 4.1 and 4.2 show that the oxidized steels can be ranked according to the weight gain (higher to lower) as; P-11, C-5, P-22 and P-5 respectively at both temperatures. Figure 4.3 shows the amount of weight gain and the effect of temperature on the weight gain for all steels at the end of 48 hours of oxidation.
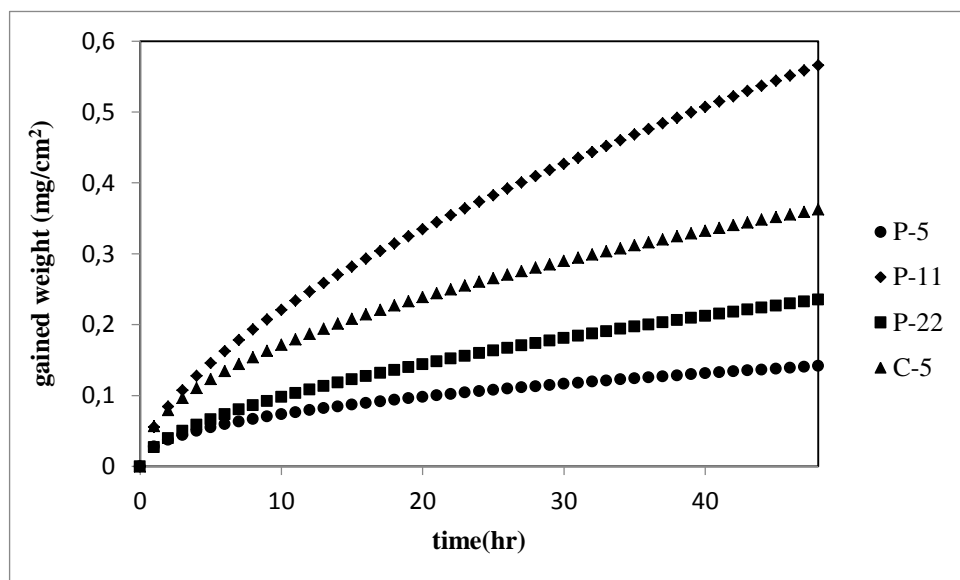
Figure 4.1 The weight gain during oxidation of the four steels at 450°C in air
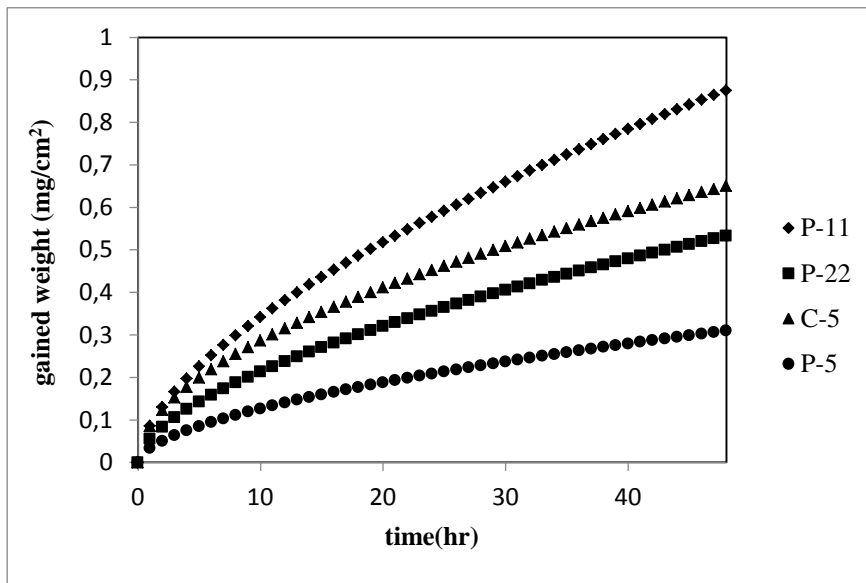
Figure 4.2 The weight gain during oxidation of the four steels at 500°C in air

The results of the weight gain for tests done at 500°C were higher than those done at 450°C and this was expected since the diffusion of species that control the oxidation process is faster at higher temperatures.
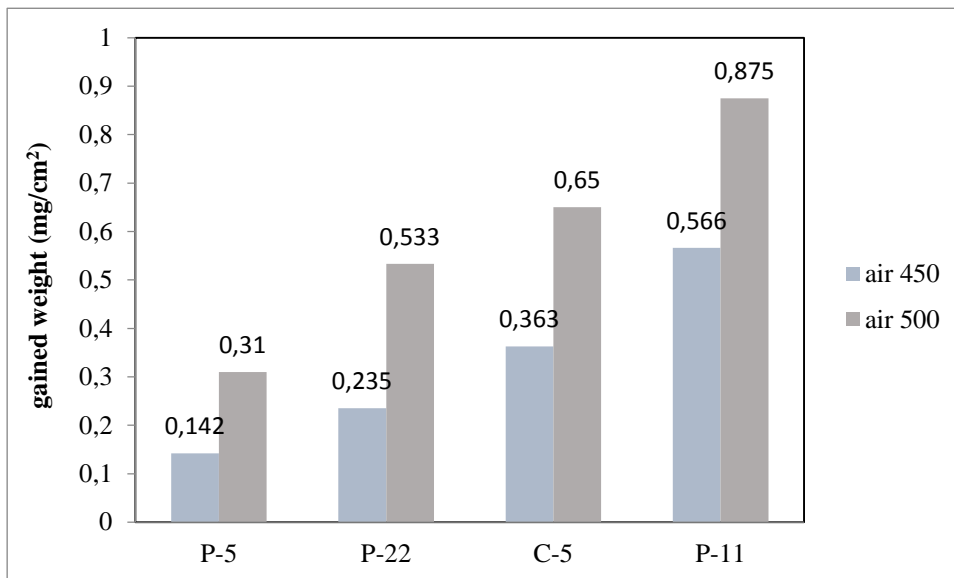
Figure 4.3 The weight gain of the four steels in air at 450 and 500°C at the end of 48 hours of oxidation

By looking at the Table 3.1, the above results can only be related to chromium contents of P-5, P-22 and P-11 since the weight gain increases as chromium content decrease. The lower weight gain in the case of C-5 relative to P-11 steel maybe related to the difference in the carbon, manganese and silicon contents in these steels.

4.3 Oxidation in $CO_2+N_2+H_2O$ Atmosphere

The thermogravimetric test results of oxidation of the four steels in $CO_2+N_2+H_2O$ environment at two different temperatures are shown in Figures 4.4 and 4.5. In this environment, the weight gain was higher than that of air for all steels and the steels ranking was different since C-5 steel gained the lowest weight and then come P-22, P-11 and P-5 with the highest weight gain.
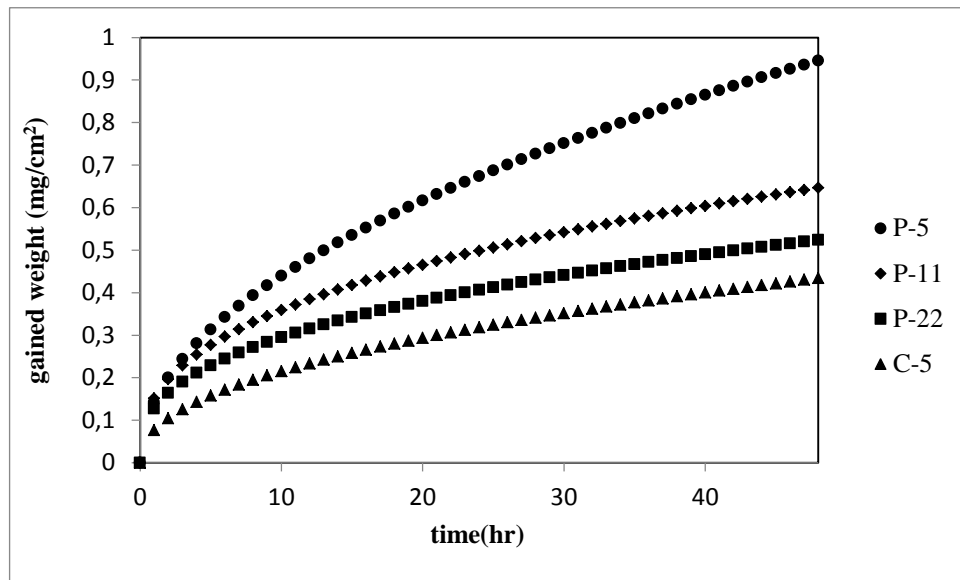
Figure 4.4 The weight gain during oxidation of the four steels in $CO_2+N_2+H_2O$ at 450°C

After 48hrs oxidation period, the amounts of gained weights for the four steels at the two temperatures are given in Figure 4.6. Again from the same figure we can see the effect of temperature on the oxidation behavior of the steels and as expected all the steels were oxidized more at the higher temperature.
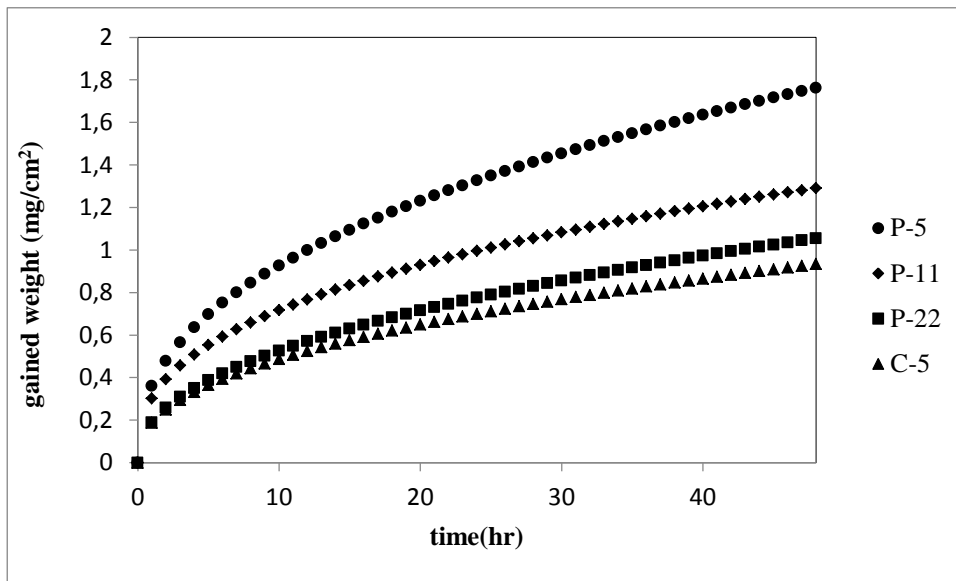
Figure 4.5 The weight gain during oxidation of the four steels in $CO_2+N_2+H_2O$ at 500°C

From the correlation of results given in Figures 4.4 and 4.5 with compositions given in Table 3.1, contrary to the weight gain in air oxidation, the weight gain generally increased as the chromium content increased. This was evidently shown since C-5 steel that does not contain any chromium gained the lowest weight among the other steels; P-5, P-11 and P-22.
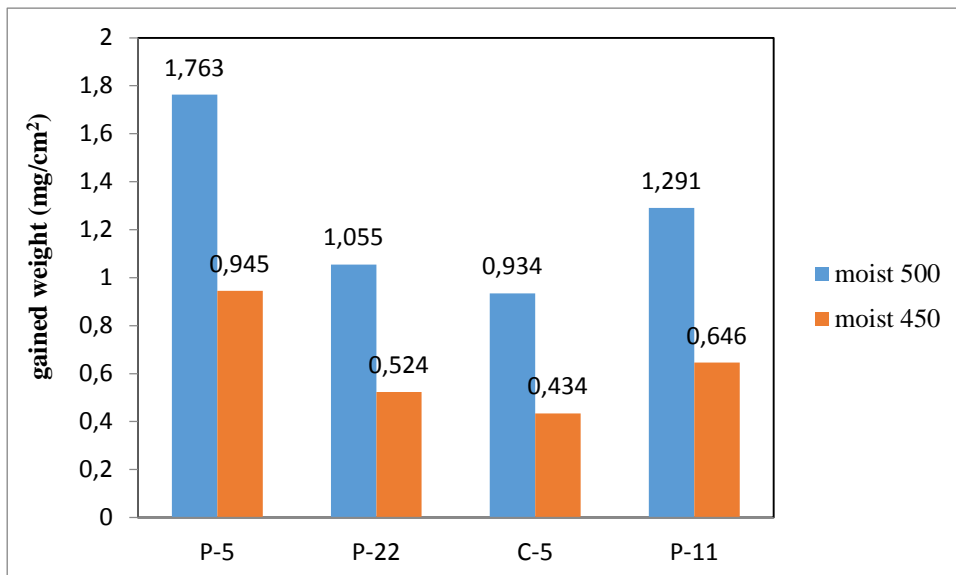
Figure 4.6 The weight gain of the four steels in $CO_2+N_2+H_2O$ at 450 and 500°C at the end of 48 hours of oxidation

To summarize the above findings, Figure 4.7 and Table 4.1 were prepared. They show the weight gained for all steels in (mg/cm^2) in both environments at two temperatures at the end of 48 hours of oxidation.
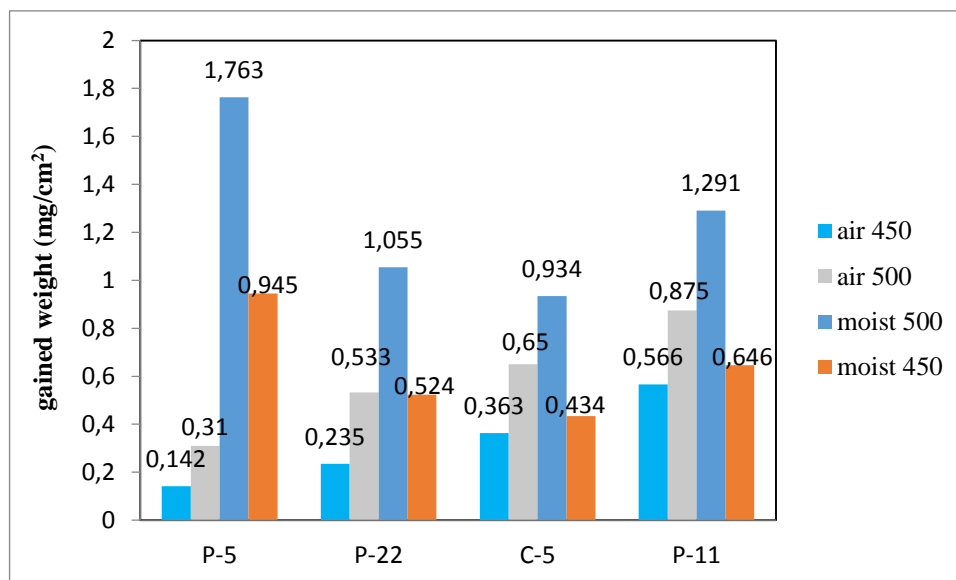
Figure 4.7 The weight gain of the four steels in air and CO_2+N_2+H_2O at 450 and 500°C at the end of 48 hours of oxidation

Table 4.1 Weight gain after 48-hour oxidation period in air and in CO_2+N_2+H_2O gas mixture at two temperatures

Steel	Weight gained in air for 48 hr in (mg/cm^2)				Weight gained in CO_2+N_2+H_2O for 48 hr in (mg/cm^2)			
	450°C		500°C		450°C		500°C	
	W.gain	*S_e	W.gain	*S_e	W.gain	*S_e	W.gain	*S_e
C-5	0.363	58x10^{-4}	0.65	6.7x10^{-4}	0.434	13x10^{-4}	0.934	48x10^{-4}
P-22	0.235	7x10^{-4}	0.533	22.5x10^{-4}	0.524	45x10^{-4}	1.055	41x10^{-4}
P-11	0.566	30x10^{-4}	0.875	42x10^{-4}	0.646	97x10^{-4}	1.291	99x10^{-4}
P-5	0.142	4.3x10^{-4}	0.31	17x10^{-4}	0.945	23x10^{-4}	1.763	68x10^{-4}

*S_e: standard error of estimate

From above results, it was seen that the environments containing H_2O and CO_2 gases were more corrosive since the corrosion rate was higher than that in air. To identify whether this high corrosivity was due to the presence of water vapor or carbon dioxide, oxidation of P-5 steel in two different gas mixtures of 15% H_2O+85%N_2 and 15%CO_2+85%N_2 at 500°C was done and the results are shown in Figure 4.8 below. To observe the effect of gas phase clearly, P-5 steel was chosen because it had the highest concentration of chromium among the four steels studied and showed the largest difference in weight gain when gas phase was

changed. As it can be seen in Figure 4.8, presence of water vapor in gas phase was more effective than CO_2 in oxidation of P-5 steel.
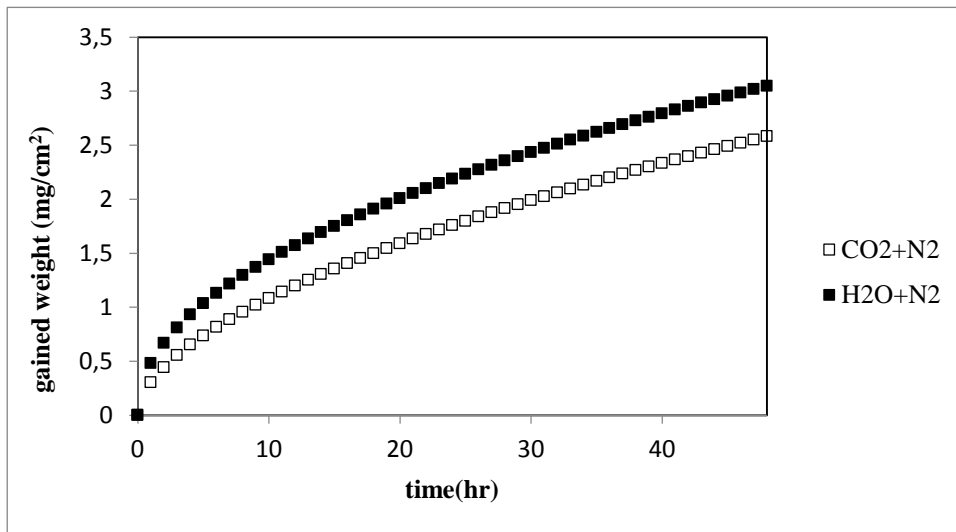
Figure 4.8 The weight gain during oxidation of P-5 steel in 15%CO_2+85%N_2 and 15%H_2O+85%N_2 at 500°C

To verify that the increase in oxidation rate in gas phase containing water vapor was caused by structural modification of hydrogen, P-5 steel was subjected to hydrogen charging before oxidation in air. Again, to observe the effect of hydrogen charging clearly, P-5 steel was chosen because it had the highest concentration of chromium among the four steels studied. Figure 4.9 shows the results of P-5 steel oxidized in air at 500°C. To show the effect of hydrogen charging prior to oxidation in air, result of oxidation in air without hydrogen charging was repeated here. As it can be seen in Figure 4-9, charging the steel by hydrogen prior to oxidation in air increased the rate of oxidation of P-5 steel.
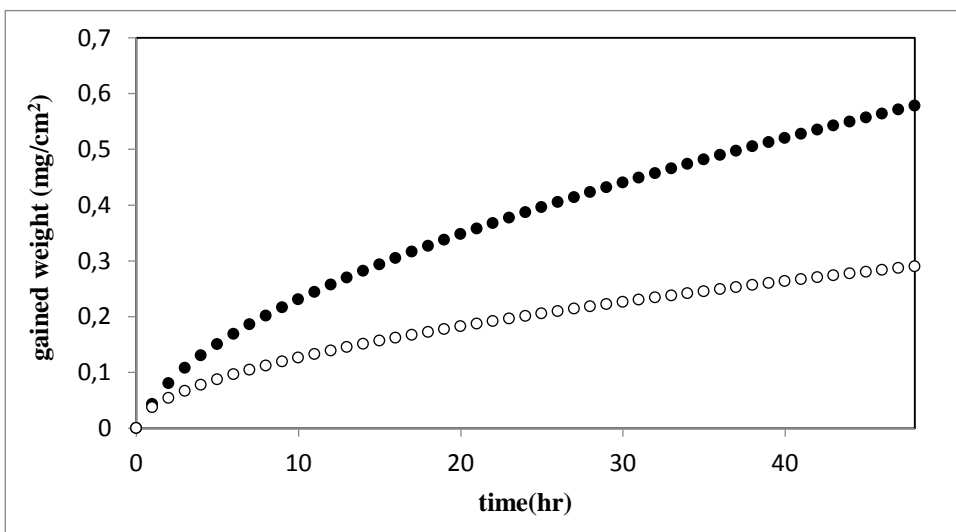
Figure 4.9 The weight gain during oxidation of hydrogen charged (●) and non-charged (○) P-5 steel samples in air at 500°C

4.4 Introduction of Free Oxygen

From the comparison of results, oxidation by O_2 in air and H_2O in combustion products, it was seen that oxidation by O_2 was slower. Therefore, free oxygen was introduced to water vapor containing simulated combustion gas to examine the reducing effect of free oxygen on the rate of oxidation. By this way, formation of protective chromium containing oxide was expected to passivate the surface of the steel. The effect of free oxygen on the rate of oxidation was also studied by testing P-5 steel that had the highest concentration of chromium among the four steels studied. It was expected that the passivation effect maybe observed more easily in this steel because it showed the largest difference in weight gain when gas phase was changed. The tests were performed at $500^{o}C$ and the gas composition can be represented by $XO_2+2H_2O+7.52N_2$ where, X has values of 3 and 8. This provides two different R values (R= the ratio of H_2O to O_2 partial pressures = 2/X). The weight gain data during oxidation are shown in Figure 4.10. The weight gain during oxidation of P-91 steel in 21% H_2O + 79% N_2 was used to compare the effect of introducing free oxygen on the corrosion rate of P-5.
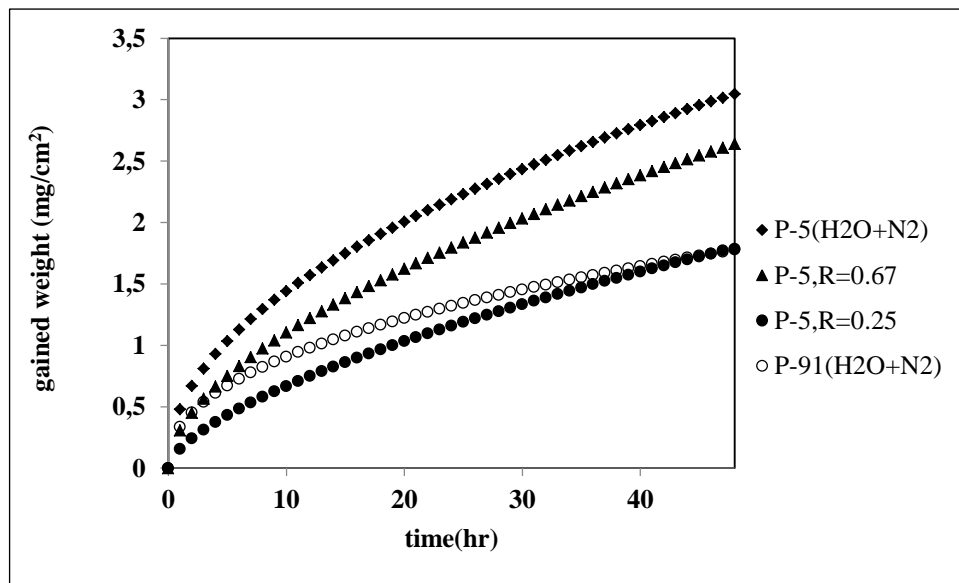
Figure 4.10 The weight gain during oxidation of P-5 and P-91 steels in different gas compositions at $500^{o}C$

Getting the above result has led us to consider that it could be useful to extend the oxidation of P-5 steel at $500^{o}C$ in gas mixtures of N_2, O_2 and H_2O with different compositions and construct A $(0.21H_2O+0.79Air)$ - B (Air) - C $(0.21H_2O+0.79N_2)$ composition triangle. By this way the effect of excess air on oxidation rate of P-5 steel can be determined. The minimum number of composition points was calculated and given in Table 3.3. The distribution of these points on the composition triangle was shown in Figure 3.3. The weight gain data measured at different R values, where R value is changing from point to point on the composition triangle, is given in appendix A.

Figure 4.11 shows the output of the minimal factor program indicating the regions of weight gain for P-5 steel in environments corresponding to gas compositions represented by the composition triangle at the end of 48 hours of oxidation at 500°C. Figure 4.12 was constructed as the weight gain of P-5 steel versus R (P_{H2O}/P_{O2}) after 48 hrs of oxidation period in different gas mixtures that are represented by ten points used to construct Figure 4.11.

From Figures 4.11 and 4.12 it can be seen that, introduction of free oxygen to H_2O containing environments reduces the rate of oxidation. There is a drastic decrease in oxidation rate when the gas phase composition changes from 0.21 H_2O + 0.79 N_2 composition to R=2.62. The first composition could simulate the combustion product of hydrogen with theoretical amount of air diluted by nitrogen; the later corresponds to the same combustion product containing about 25 % excess air. Nearly 30 % reduction in rate of oxidation was achieved when about 25 % excess air was used in the combustion. From this composition to R = 1 or even below 1, corresponding to about 100 % or more excess air in the combustion of hydrogen does not show any significant change in the oxidation rate of P-5 steel. Further decrease in R again decreases the oxidation rate drastically.
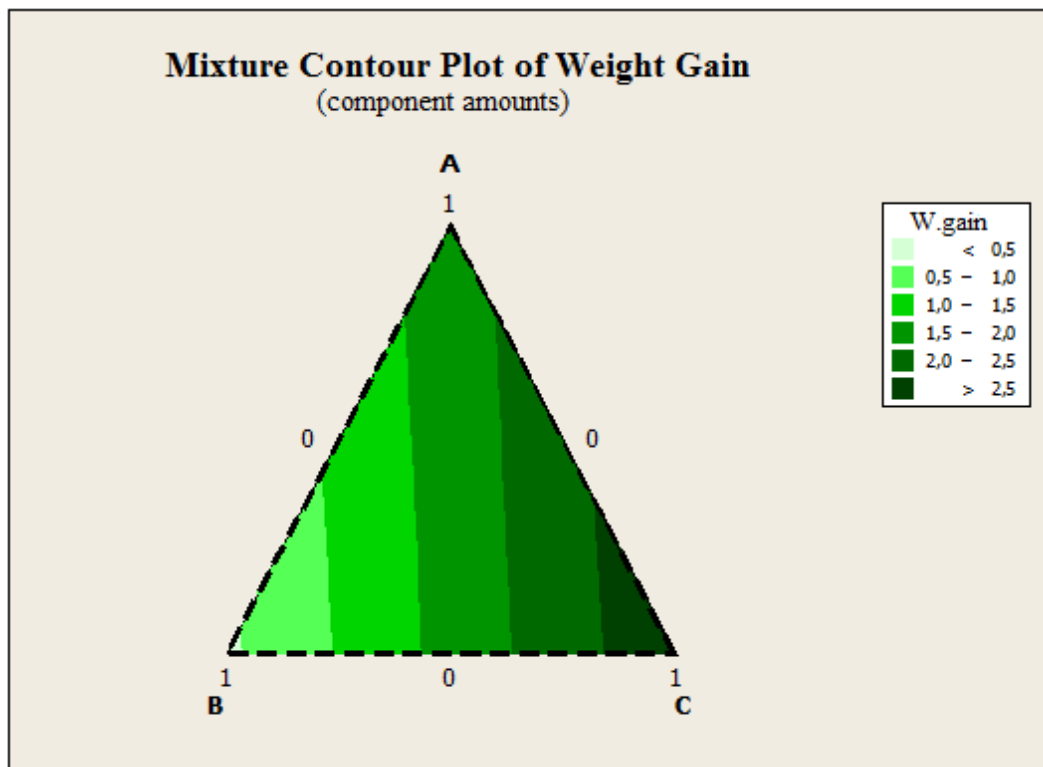
Figure 4.11 The regions of weight gain of P-5 steel at the end of 48 hours of oxidation at 500°C in gas phase represented by A (0.21H$_2$O+0.79Air) – B (0.21O$_2$+0.79N$_2$) – C (0.21H$_2$O+0.79N$_2$) composition triangle
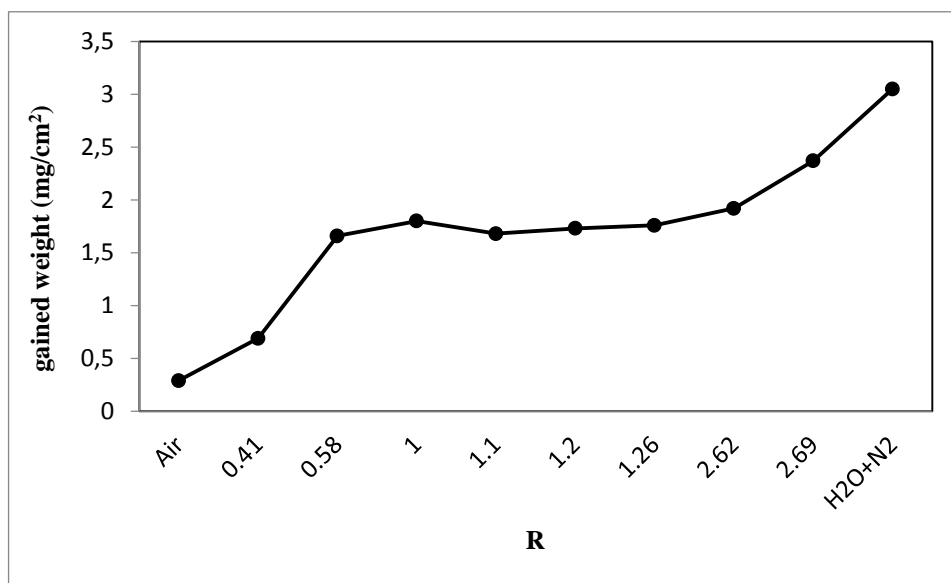
Figure 4.12 Weight gain vs. R for the points represented in the composition triangle

4.5 Analysis of Oxidation Products

To explain the TG oxidation results and to identify the formed oxides, further tests like X-ray diffraction and microscopic analysis were performed on oxidized samples. The X-ray diffraction patterns given through Figures 4.13 - 4.18 show the presences of M_2O_3 and M_3O_4 type oxide peaks and Fe peaks in some cases. The X-ray diffraction patterns of samples are presented to show the effect of the oxidizing gas environment on the oxidation products formed.
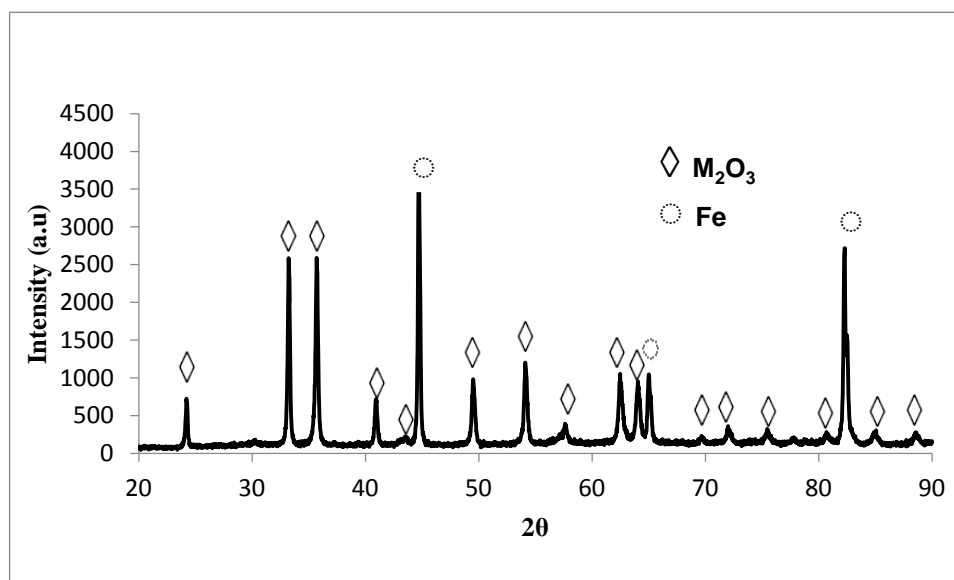
Figure 4.13 X-ray diffraction pattern of P-5 oxidized in air at 500°C
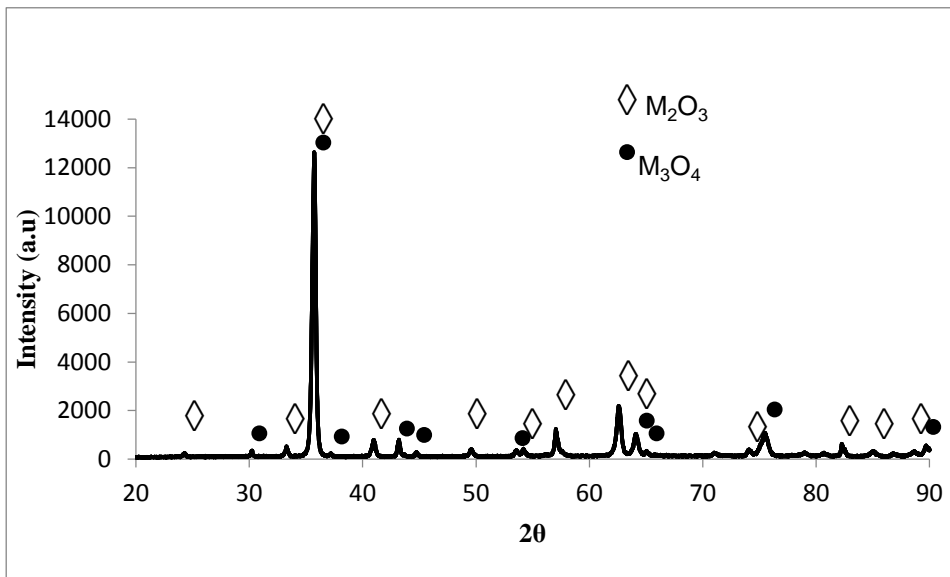
Figure 4.14 X-ray diffraction pattern of P-5 oxidized in $CO_2+N_2+H_2O$ at 500^oC
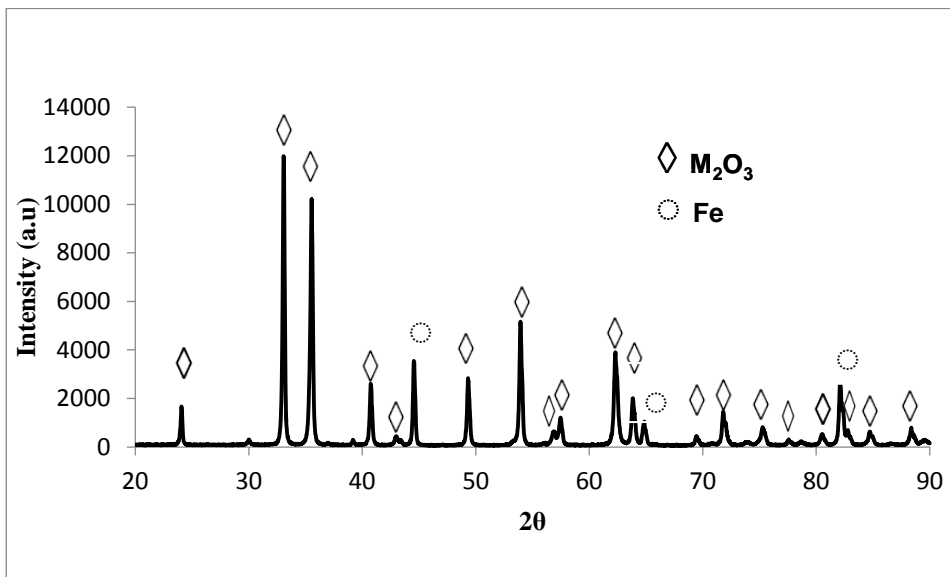
Figure 4.15 X-ray diffraction pattern of P-22 oxidized in air at 500^oC
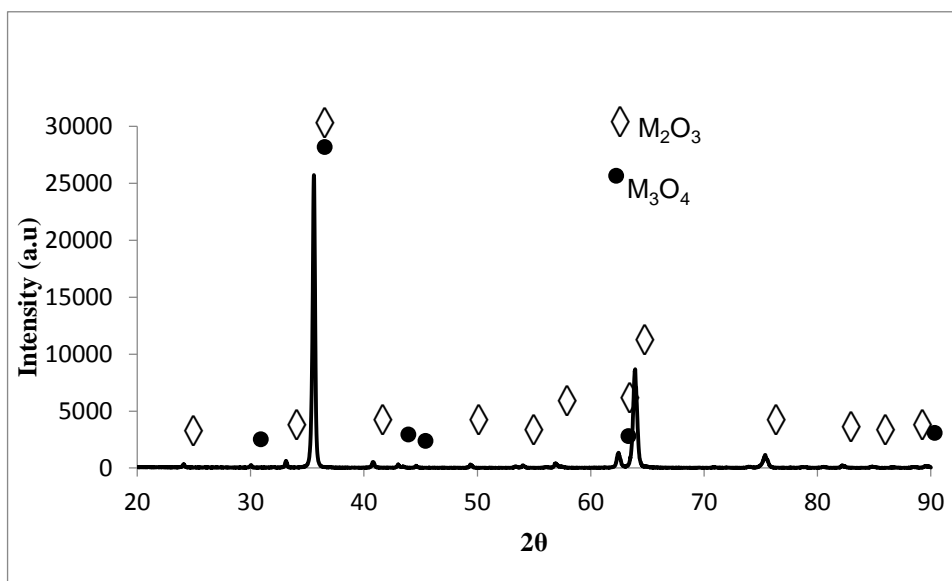
Figure 4.16 X-ray diffraction pattern of P-22 oxidized in CO_2+N_2+H_2O at 500°C
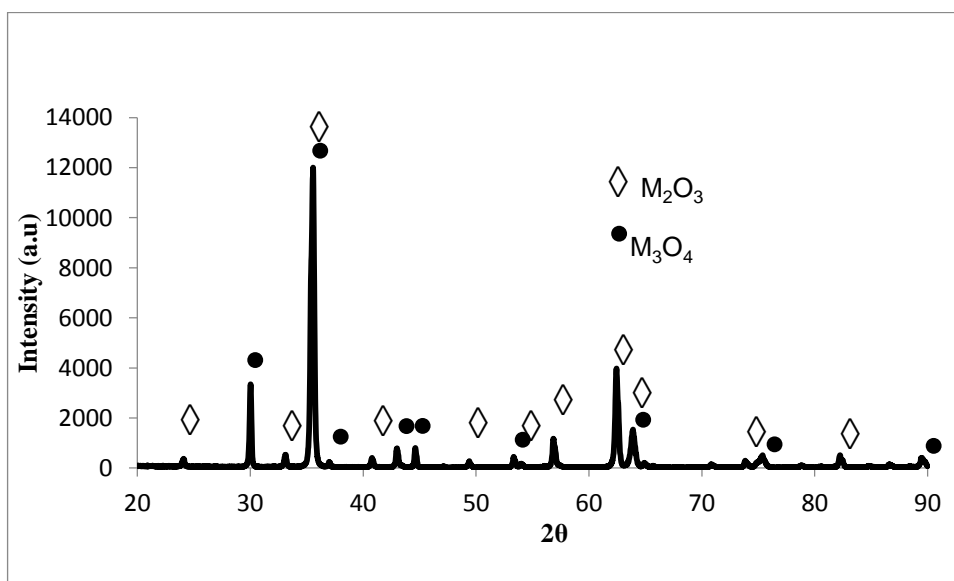
Figure 4.17 X-ray diffraction pattern of P-11 oxidized in CO_2+N_2+H_2O at 450°C
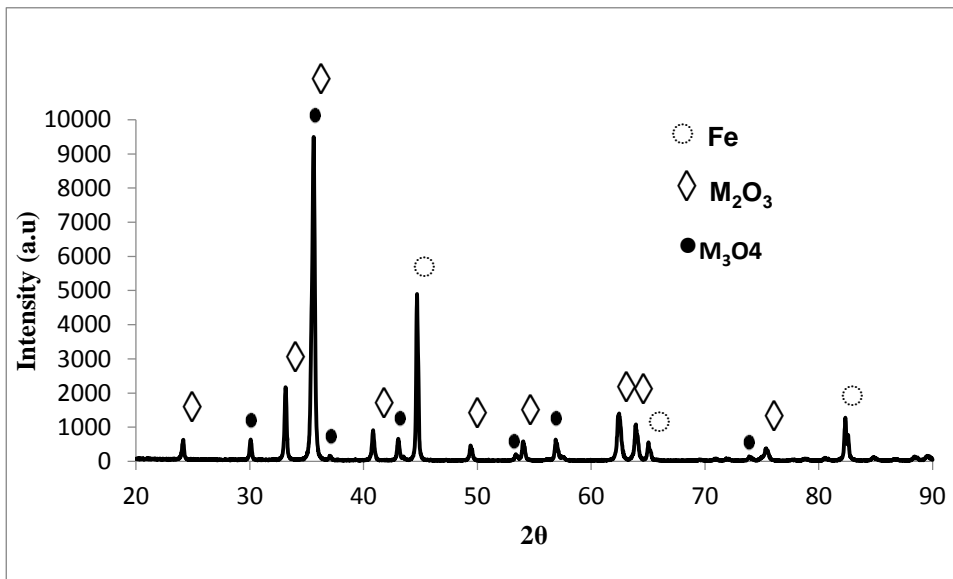
Figure 4.18 X-ray diffraction pattern of C-5 oxidized in air at 450°C

Examination of X-ray diffraction results of all steels showed the formation of M_2O_3 and M_3O_4 type of oxides where M may be; Fe, Cr or Fe-Cr. In the presence of water vapor, the intensities of peaks are higher and that explained as both M_2O_3 and M_3O_4 present and their peaks are imposed on each other. Fe peaks are believed to be coming from steel samples under oxide films in air oxidation.

Optical microscope study for the oxidized samples showed two distinguished (darker color tone of Fe_3O_4 relative to Fe_2O_3) oxide layers of Fe_3O_4 and Fe_2O_3 (see Figures 4.19 through 4.21). The examination of these images showed that an inner layer of Fe_3O_4 at the metal/oxide interface and a thin outer layer of Fe_2O_3 at the gas/oxide interface. Assuming that only Fe_2O_3 and Fe_3O_4 are the oxidation products, approximate relative thicknesses of oxide phases used in the calculation of the approximate weight of metal loss as given in Appendix B can be calculated from the optical photographs.
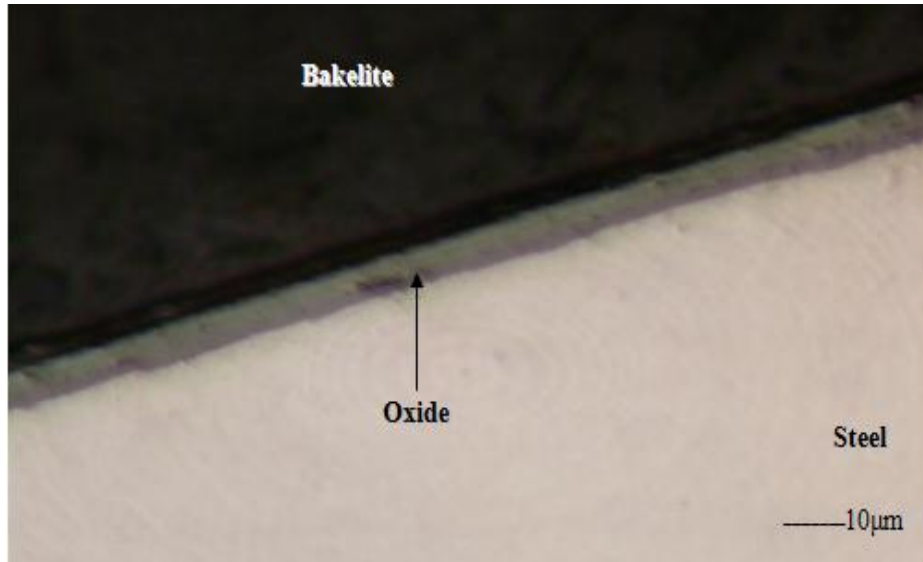
Figure 4.19 Optical photograph of C-5 steel oxidized at 450°C in $CO_2+N_2+H_2O$ (200X)
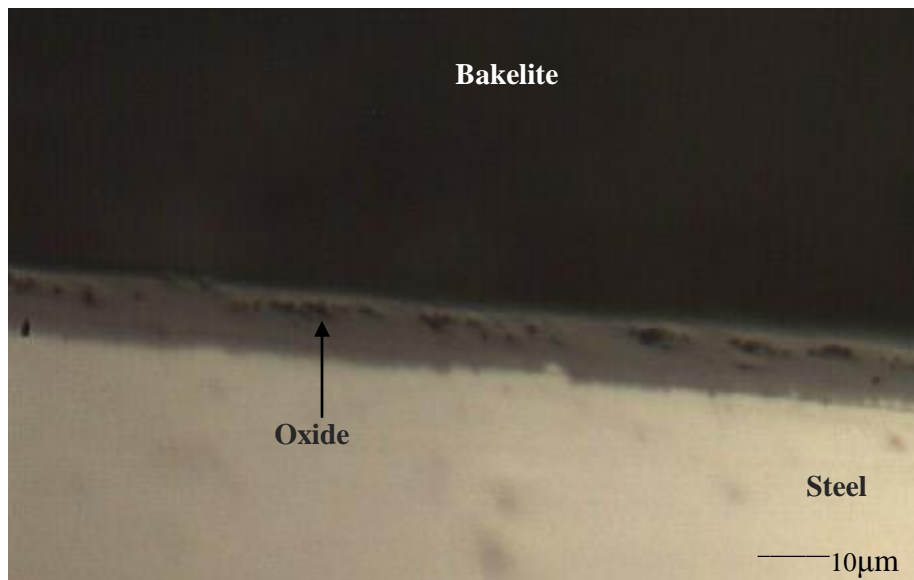
Figure 4.20 Optical photograph of P-5 steel oxidized at 500°C in $CO_2+N_2+H_2O$ (500X)
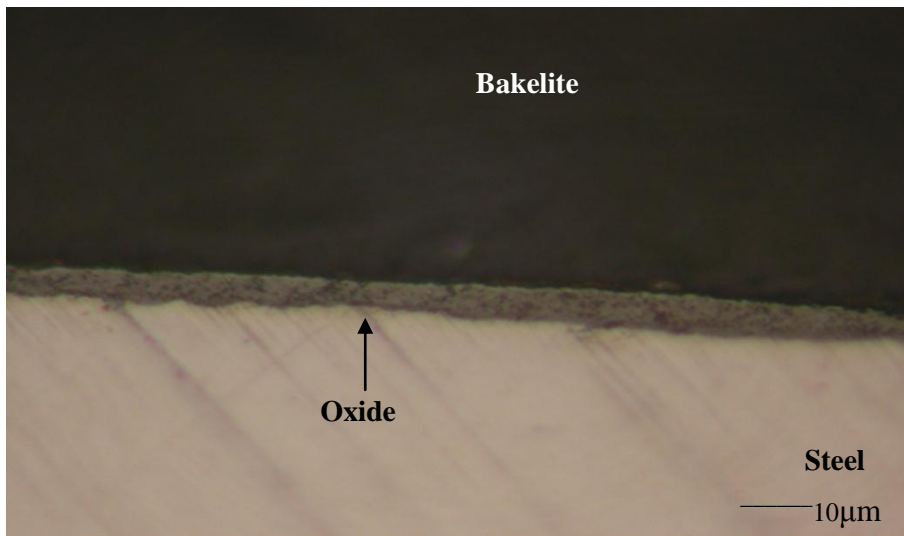
Figure 4.21 Optical photograph of P-11 steel oxidized at 450°C in air (200x) [61]

To get information about the morphology and to identify the formed oxides, SEM analyses (elemental mapping and point analysis) were performed on the oxidized samples Figures 4.22- 4.26.
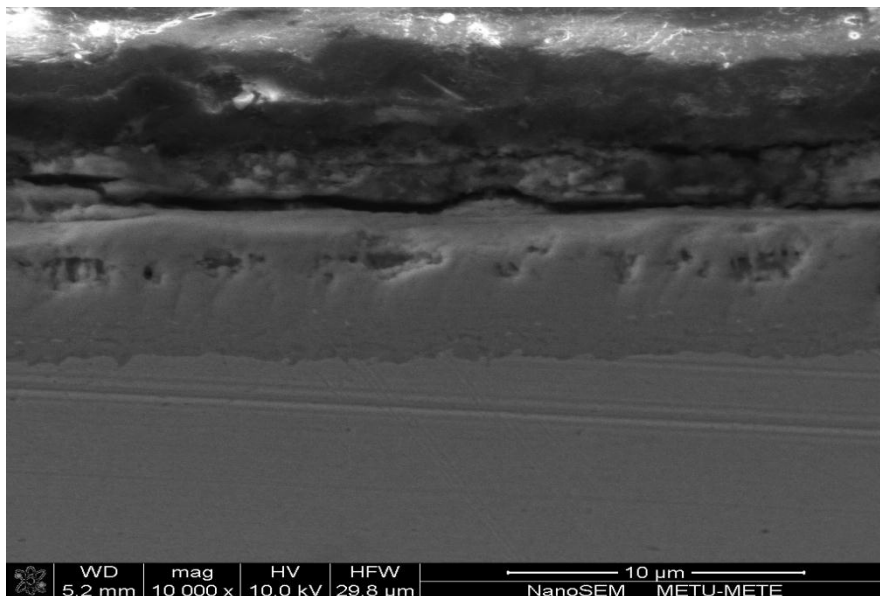
Figure 4.22 SEM micrograph of P-5 steel oxidized in $CO_2+N_2+H_2O$ at 500°C
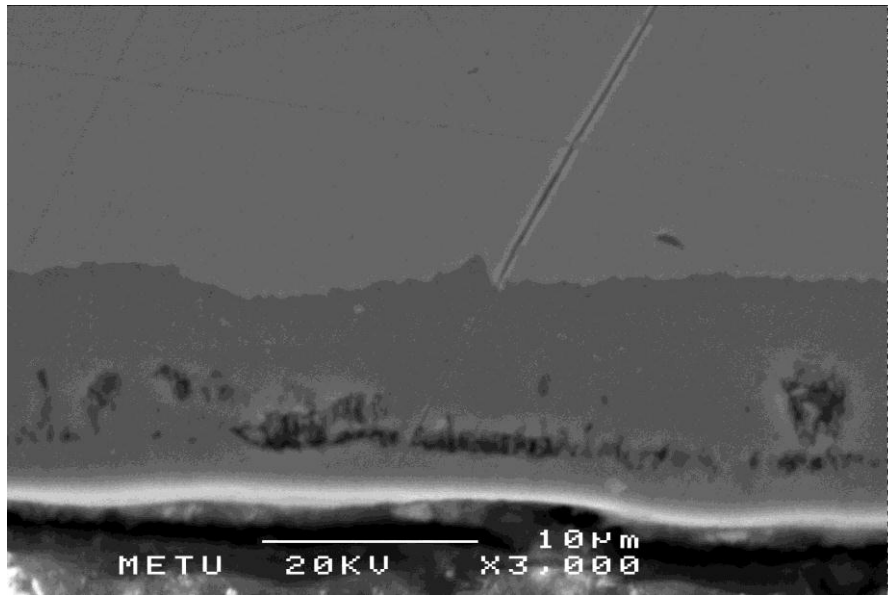
Figure 4.23 SEM micrograph of P-5 steel oxidized in CO_2+N_2 at 500°C
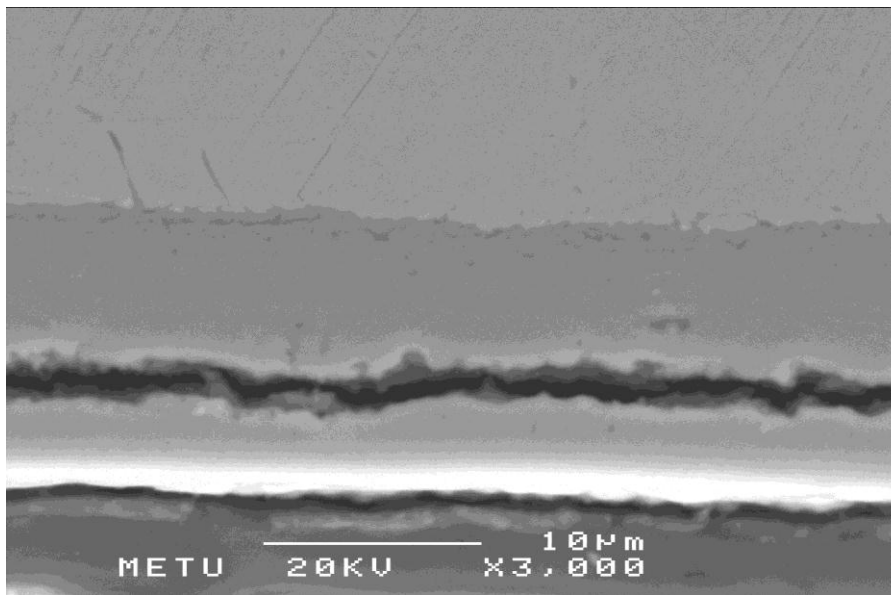
Figure 4.24 SEM micrograph of P-5 steel oxidized in H_2O+N_2 at 500°C
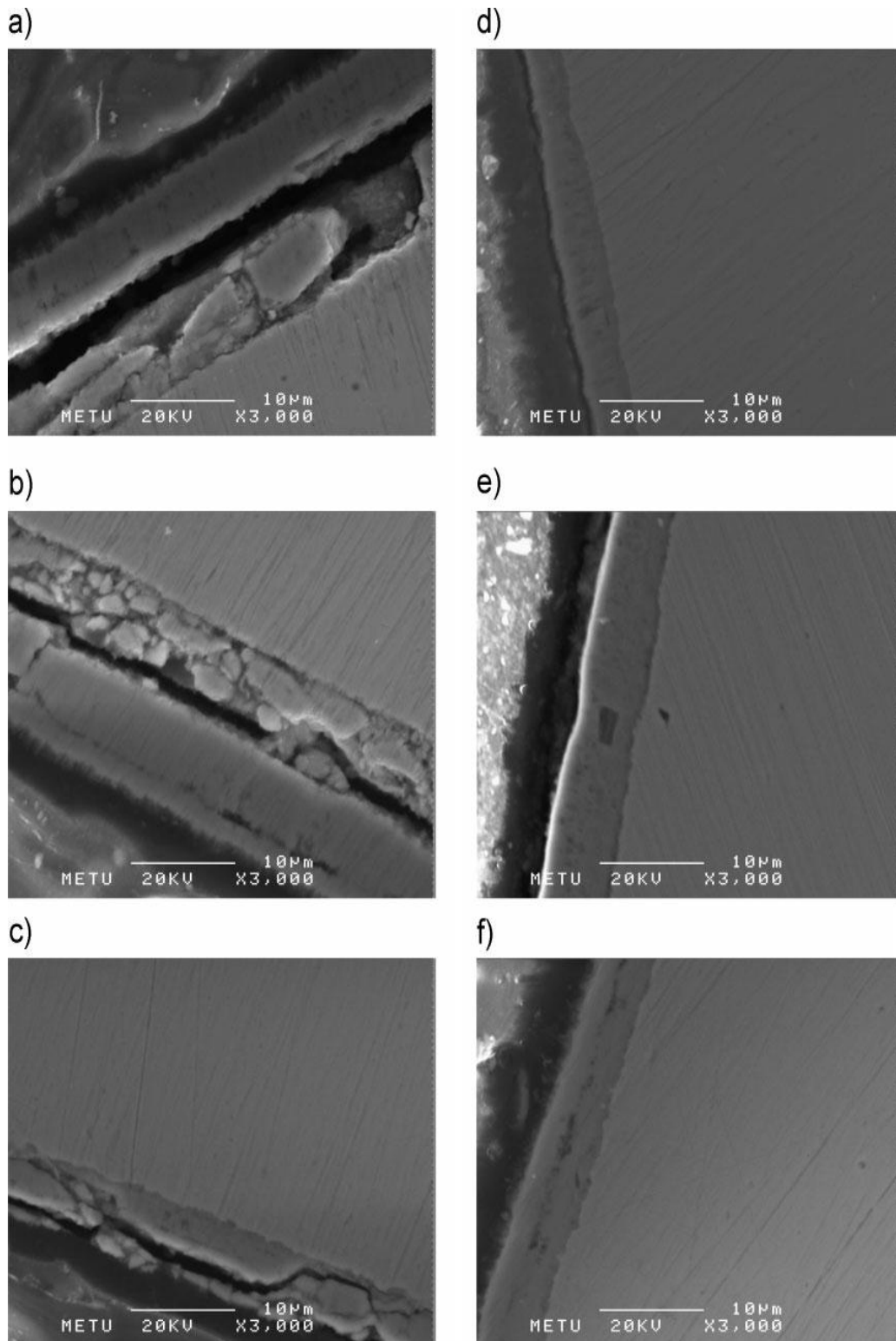
Figure 4.25 SEM micrograph of (a) C-5, (b) P-11 and (c) P-22 steels oxidized in $CO_2+H_2O+N_2$ at 500^oC. (d) C-5, (e) P-11 and (f) P-22 steels oxidized in air at 500^oC. Reproduced from [34] by the license obtained.

CHAPTER 5

DISCUSSION

The thermogravimetric results given in the previous chapter will be correlated to the kinetic models proposed for oxidation reactions in this chapter. The higher corrosion rates of steels, used in this study, in water vapor containing environments in spite of the lower oxidation potential compared to air oxidation will also be explained with reference to thermodynamic, microscopic and other considerations.

5.1 Kinetics of Oxidation

From the weight gain versus time curves given in Figures 4.1, 4.2, 4.4 and 4.5, it was seen that all steels were oxidized according to:

$$y = k * t^n \tag{5.1}$$

where 'y' is the gained weight per unit surface area in mg/cm^2, 'k' is the rate constant, 'n' is the exponent of time in the rate law and 't' is the time in hours. Presentation of ln (y) vs. ln (t) of the raw data for all steels resulted in straight lines with slopes close to 0.5 and the R^2 values (squares of the associated correlation coefficients) were greater than or equal to 0.98. Expecting that the steels oxidize following a parabolic mode, the time exponent constant (n) was forced to be 0.5 and the resulted graphs of weight gain versus $t^{0.5}$ are given in Figures 5.1 through 5.4. Table (5.1) summarized the k and R^2 values for the steels oxidized in different environments at two temperatures. From those figures and Table 5.1, it can be concluded that all steels have similar kinetic behavior in both environments at two temperatures since they all follow parabolic form during oxidation. These results support the diffusion controlled oxidation of these steels as observed in many scale formation processes [53, 62].

Table 5.1 Summary of numerical values of k and R^2 at 450 and 500°C in both environments

Steel	Air				$CO_2+N_2+H_2O$			
	k		R^2		k		R^2	
	450°C	500°C	450°C	500°C	450°C	500°C	450°C	500°C
P-5	0.019	0.043	0.99	0.99	0.134	0.221	0.99	0.99
P-22	0.036	0.082	0.99	0.99	0.054	0.145	0.98	0.99
P-11	0.092	0.124	0.99	0.99	0.083	0.134	0.98	0.98
C-5	0.051	0.107	0.99	0.99	0.06	0.102	0.99	0.99
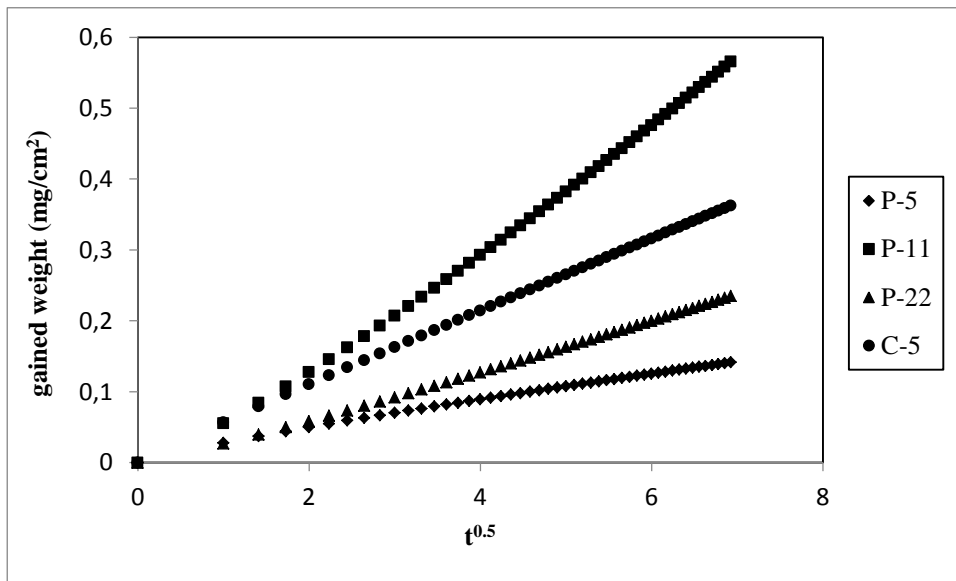
Figure 5.1 Plot of y vs. t$^{0.5}$ for all steels oxidized in air at 450°C
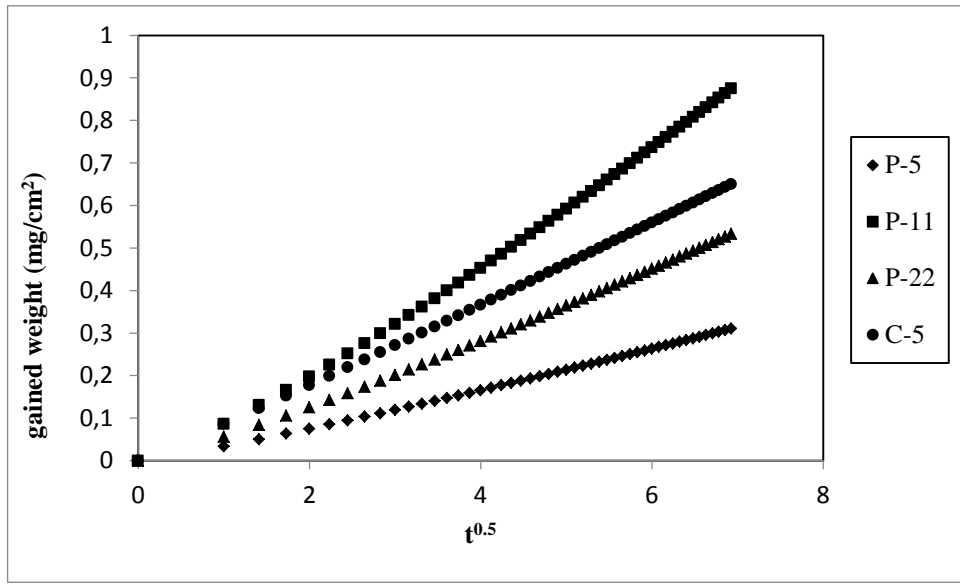
Figure 5.2 Plot of y vs. $t^{0.5}$ for all steels oxidized in air at $500^{o}C$
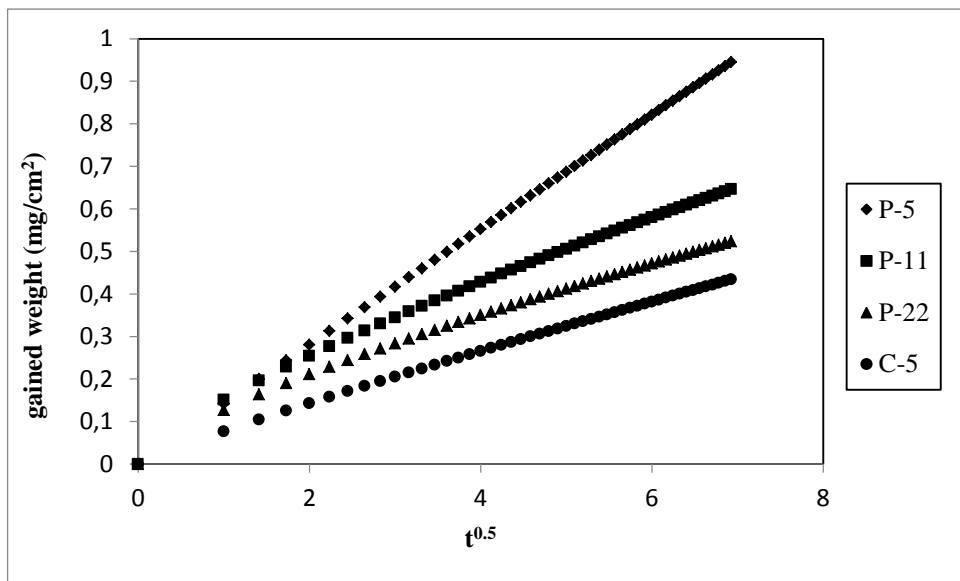
Figure 5.3 Plot of y vs. $t^{0.5}$ for all steels oxidized in $CO_2+N_2+H_2O$ at $450^{o}C$
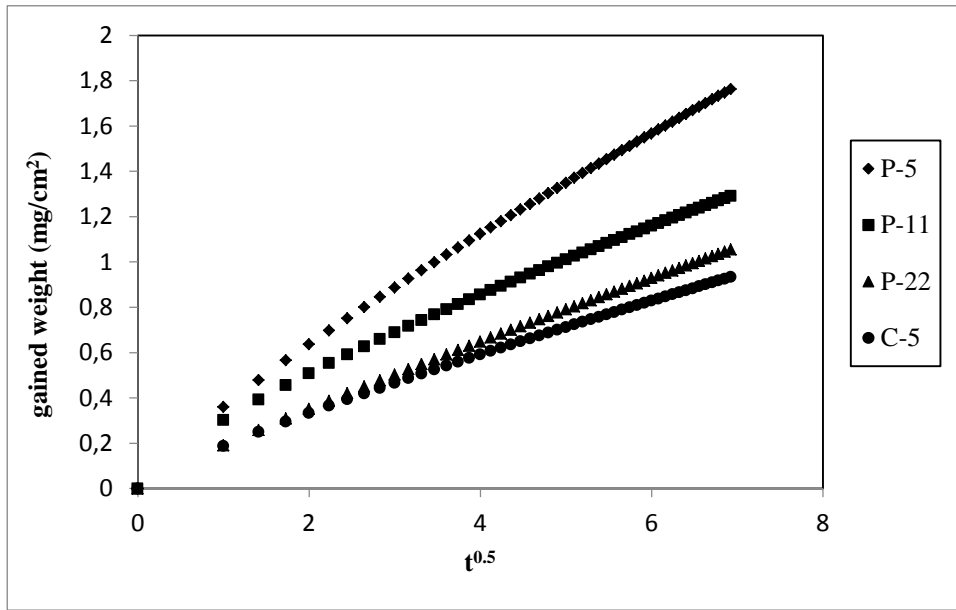
Figure 5.4 Plot of y vs. $t^{0.5}$ for all steels oxidized in $CO_2+N_2+H_2O$ at 500°C

5.2 Thermodynamic Consideration

Among the steels used in this study, P-5 steel gained the lowest weight in air oxidation because it indicated better oxidation resistance due to higher chromium content relative to the other steels. Thermodynamic computations along with structural information of the oxide phase may be used to explain this observation. Equilibrium computations given in APPENDIX C show that during oxidation in air at 450 and 500°C temperatures, the stable form of iron oxides was Fe_2O_3 [63] as a result of the direct contact of iron with oxygen according to the following reaction:

$$2Fe + 3/2O_2 \rightarrow Fe_2O_3 \tag{5.2}$$

The reaction of the formed Fe_2O_3 with Fe supplied from the base steel results in formation of Fe_3O_4 at the interface between Fe_2O_3 and Fe (reaction 5.3).

$$4Fe_2O_3 + Fe \rightarrow 3Fe_3O_4 \tag{5.3}$$

This formed Fe_3O_4 reacts with oxygen from the air at Fe_2O_3/Fe_3O_4 interface and be converted to Fe_2O_3 according to:

$$2Fe_3O_4 + 1/2O_2 \rightarrow 3Fe_2O_3 \tag{5.4}$$

Fe_3O_4 layer is grown continuously as a result of the interaction of Fe coming from steel with Fe_2O_3 at Fe_2O_3/Fe_3O_4 interface (reaction 5.3).

On the other hand, under the conditions covered in this study, thermodynamic equilibrium computations given in APPENDIX C [63] showed that Fe_3O_4 was the stable iron oxide

during oxidation in H_2O and/or CO_2 containing environments according to reaction (5.5) and this result was confirmed by A. Rahmel et al. [64].

$$3Fe + 4CO_2 \rightarrow Fe_3O_4 + 4CO$$

(5.5)

$$3Fe + 4H_2O \rightarrow Fe_3O_4 + 4H_2$$

(5.6)
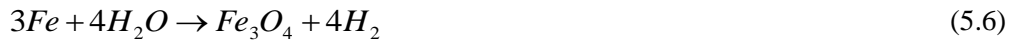
Further oxidation of Fe_3O_4 by CO_2 from the environment resulted in formation of Fe_2O_3 according to:

$$2Fe_3O_4 + CO_2 \rightarrow 3Fe_2O_3 + CO$$

(5.7)

$$2Fe_3O_4 + H_2O \rightarrow 3Fe_2O_3 + H_2$$

(5.8)

Growth of Fe_3O_4 layer continues as a result of reaction 5.3 and 5.5 at Fe_3O_4/Fe_2O_3 and Fe/Fe_3O_4 interfaces respectively. Figure 5.5 shows the sequence of oxide formation and the diffusing species during oxidation of iron.
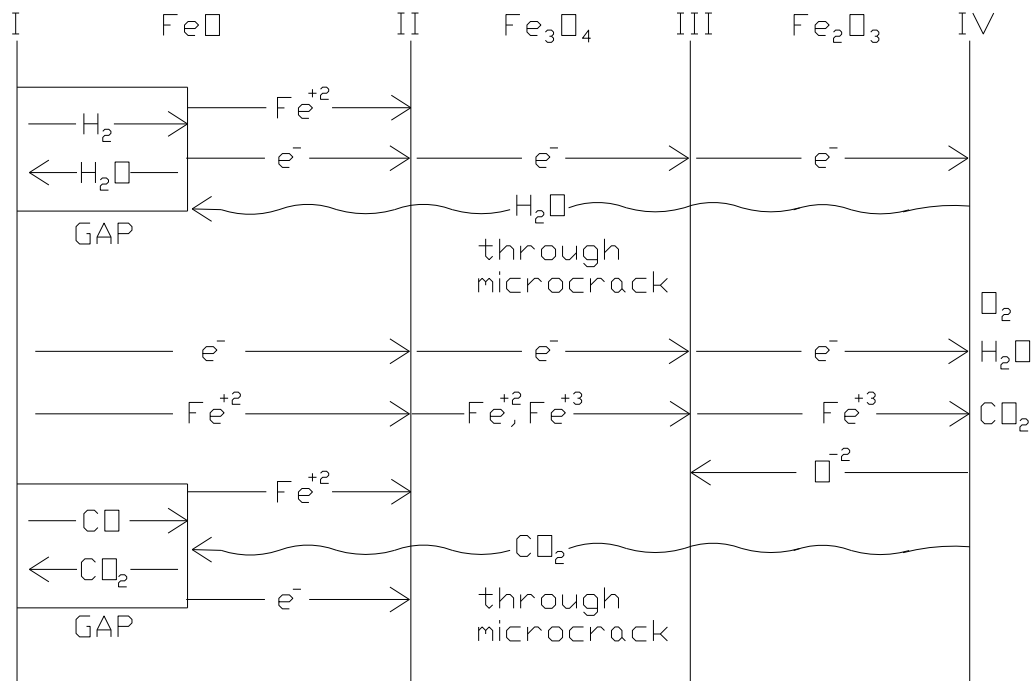
Figure 5.5 Mechanism of the oxidation of iron in atmospheres containing H_2O and CO_2 as suggested by Rahmel and Tobolski [64]

Therefore, the low weight gain of P-5 (5%Cr) and P-22 (2.25%Cr) in air oxidation was believed to be related to the capability of these steels to form a protective layer rich in Cr on the surface (see Figures 5-5 and 5-6). This layer might have slowed down the Fe diffusion to

some extent and reduced the Fe_3O_4 formation and the result was lower corrosion rate in the air.

5.3 Microscopic and Other Considerations

SEM analyses were done to understand the local constitution of phases that are formed on steel surfaces and drive conclusions from the thermogravimetric results. The examination of the SEM micrographs given in Figures 4-25 for the oxidized steels indicated that the scales formed on steels which gained lower weight in both environments were less porous compared to the scales in other cases and this may explain the lower corrosion rate of those steels. The formation of pores was commonly seen inside the scales formed during oxidation in the presence of water vapor and/or carbon dioxide and in some cases a continuous gap between the metal and oxide and/or between the oxide layers could be seen. In water vapor and carbon dioxide containing environments, these gases react according to reactions 5.5 - 5.6 to form oxides by providing gaseous species like H_2 and CO that may accumulate inside the pores and cause crack of the scale. Therefore, the oxidant gases will find easier paths to penetrate through those cracks and reach the steel surface and expedite oxidation.
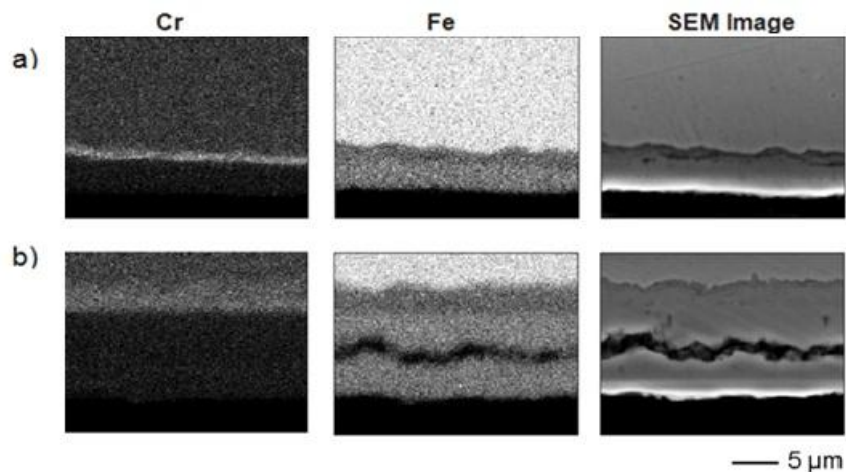
Figure 5.6 Elemental distribution maps of Cr and Fe together with SEM images after 48 hrs of P-22 steel oxidized (a) in the air and (b) in $CO_2+H_2O+N_2$ at 500°C. Reproduced from [34] by the license obtained.

48
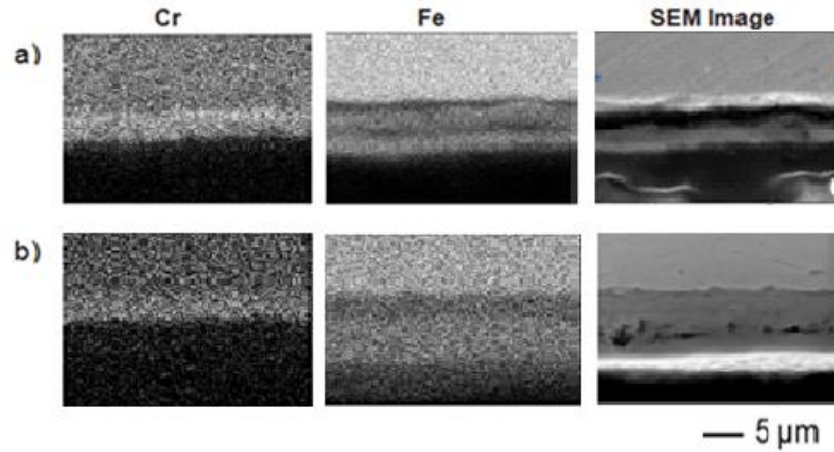
Figure 5.7 Elemental distribution maps of Cr and Fe together with SEM images after 48 hrs of P-5 steel oxidized (a) in the air and (b) in $CO_2+H_2O+N_2$ at 500°C.

In addition to the crack and pore formations during oxidation in the presence of water vapor and/or carbon dioxide, the higher corrosion rate for P-5 and P-22 steels compared to C-5(0%Cr) steel can be attributed to the loss of the protective effect of Cr in the oxide layer that is just over the surfaces of steels. Different mechanisms proposed to explain this behavior were given in section 2.4. One of them was diminishing of the protective Cr_2O_3 layer as a result of its reaction with water vapor and oxygen forming a volatile chromium-oxide-hydroxide ($CrO_2(OH)_2$) according to:

$$1/2\,Cr_2O_3 + H_2O + 3/4\,O_2 \rightarrow CrO_2(OH)_2 \qquad (5.7)$$

From the thermodynamic data of Opila [44], the standard Gibbs energy change (ΔG^o) for the above reaction can be calculated as:

$$\Delta G^o(j) = 53,500 + 45.5*T(K) \qquad (5.8)$$

The calculation of ΔG^o yielded 86.396 kj and 88.671 kj at 450 and 500°C, respectively. At equilibrium, it is given by,

$$\Delta G^o = -RT \ln(\frac{P_{CrO_2(OH)_2}}{P_{H_2O}*P_{O_2}^{3/4}}) \qquad (5.9)$$

From rearrangement of eq.5.9 the equilibrium partial pressure of chromium-oxide-hydroxide ($P_{CrO2(OH)2}$) can be obtained as:

$$P_{CrO_2(OH)_2} = e^{(-\Delta G^o/RT)}*P_{H_2O}*P_{O_2}^{3/4} \qquad (5.10)$$

When oxygen partial pressures of 2×10^{-11} and 1.18×10^{-10} [63] atmosphere at 450 and 500 ^{o}C, calculated from $CO_2+H_2O+N_2$ gas mixture equilibria, were used to calculate equilibrium

partial pressures of $CrO_2(OH)_2$ at above temperatures; $1.13x10^{-15}$ and $6.8x10^{-15}$ [44] atmosphere were determined at 450 and 500°C, respectively. These values were calculated at constant water vapor content that is equivalent to 0.19 atmosphere. Therefore, these small equilibrium partial pressure values equivalent to very low $CrO_2(OH)_2$ formation rate cannot be used to explain the higher weight gain of steel samples in water vapor containing environments. In addition, Ehlers et al. [25] found that P-91 steel with 9% Cr has gained a higher weight during oxidation in $N_2+O_2+H_2O$ gas mixture at 650°C when oxygen content decreased from 20 to 1 or 2 volume percent.

The depletion of the protective effect of chromium was also proposed to be the result of the internal oxidation of chromium instead of the formation of an external protective oxide layer. Before going further with this mechanism two separate experiments involving the use of $0.15H_2O+0.85N_2$ and $0.15CO_2+0.85N_2$ gas mixtures were done at 500°C by using P-5 steel. By this way, it was possible to distinguish the effects of H_2O and CO_2 gases, since combined effects of above gases were present in the tests performed in present study. Although the oxygen partial pressure exerted by carbon dioxide containing mixture is double that resulted from water vapor containing mixture used in these tests, Figure 4.8 shows higher oxidation rate in the presence of water vapor than that in the presence of carbon dioxide. Therefore water vapor was more effective in the development of higher weight gain which corresponds to faster oxidation of steels in $CO_2+N_2+H_2O$ environments.

Elemental maps given in Figure 5.7 show the difference in the morphology of scales formed during oxidation in different conditions. From this figure, it can be seen that the chromium distribution map in P-5 steel sample oxidized in H_2O+N_2 show the presence of a large Cr containing layer extending into the steel and supporting internal oxidation of chromium, whereas in other cases, it shows a narrow Cr concentrated layer in the oxide near the surface.
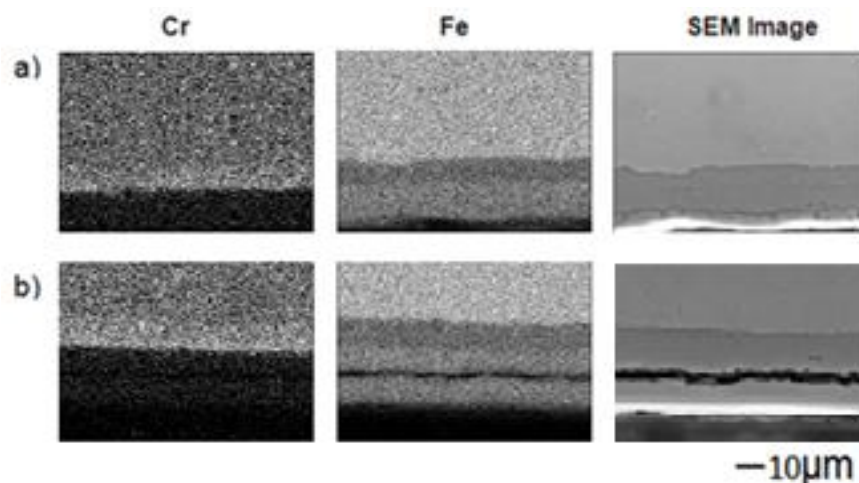
Figure 5.8 Elemental distribution maps of Cr and Fe together with SEM images after 48 hrs of P-5 steel oxidized at 500°C (a) in CO_2+N_2, (b) in H_2O+N_2

In addition, Figure 4.9 clearly shows that charging P-5 steel with hydrogen results in higher corrosion rate in air oxidation. Maud Reitveld Refinement on the x-ray diffraction results of hydrogen charged and non charged P-5 steel samples are given in Figure 5.8. From this figure it can be seen that Maud calculation showed a good fit between the raw data (blue circles) and the black line (calculated by Maud) with acceptable Rw values calculated as 10.559 and 7.0208 for hydrogen charged and noncharged respectively. Maud Reitveld Refinement calculations showed an increase in cell length (a), from 2.872 to 2.876 A^o, equivalent to 0.14% due to charging of hydrogen in to the steel. This enlargement in the lattice distance makes oxygen diffuse easier to the steel and gives an evidence that hydrogen was responsible for the internal oxidation mechanism that explain the higher weight gain in case of P-5 and P-22 steels during oxidation in water vapor containing environments.
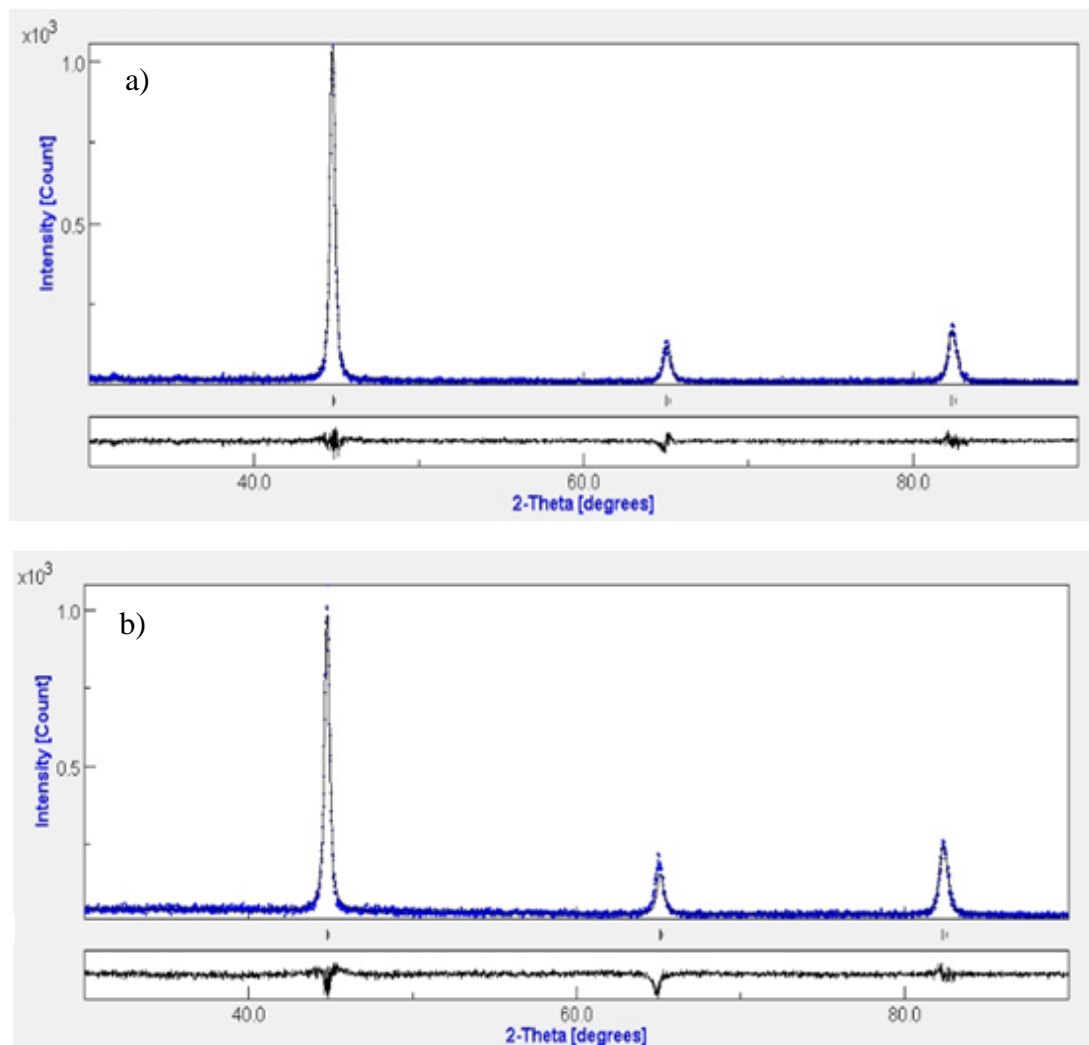
Figure 5.9 Reitveld Refinement conducted by Moud on x-ray results of (a) non charged and (b) hydrogen charged P-5 steels

To highlight the apparent higher oxidation rates of P-5 and P-22 steels in $CO_2+H_2O+N_2$ atmosphere, elemental distribution maps for P-22 and P-5 oxidized at 500^oC (a) in dry air and (b) in $CO_2+H_2O+N_2$ environment were compared in Figures 5.5 and 5.6 respectively.

From those figures, it is clear that the inner layer of the oxide next to steel was thicker in (b), but Cr was more concentrated in (a) than in (b). Furthermore, in air oxidation there was a clear interface between the oxide and the base metal meaning that the chromium rich part on the steel surface is in the oxide phase. On the other hand in $CO_2+H_2O+N_2$ environment, heavier Cr distribution seems to continue inside the steel suggesting some internal oxidation of chromium. These findings were supported by the elemental concentration profiles inside the scale extending into steel as given in Figures 5.9 and 5.10. In the case of oxidation by air a sharp increase in chromium can be seen at the steel-oxide interphase, but a gradual increase of chromium content starting from a level below the interphase extending into the oxide phase can be seen when oxide was formed by $CO_2+H_2O+N_2$ gas mixture.

From above observations, internal oxidation of chromium may be considered to be the reason of higher oxidation rates of chromium containing steels in H_2O containing environments. As a result, internal oxidation of chromium could lead to the formation of an oxide layer with less Cr than that obtained in the air due to lower mobility of the oxidized Cr in the steel.

The reason for the internal oxidation mechanism in the presence of water vapor was explained as the result of diffusion of hydrogen, provided by the oxidation reaction, through the scale into the steel and increasing the oxygen permeability of the steel [53, 65]. As a result Cr, which has lower equilibrium partial pressure of oxygen than iron can be oxidized inside the steel.
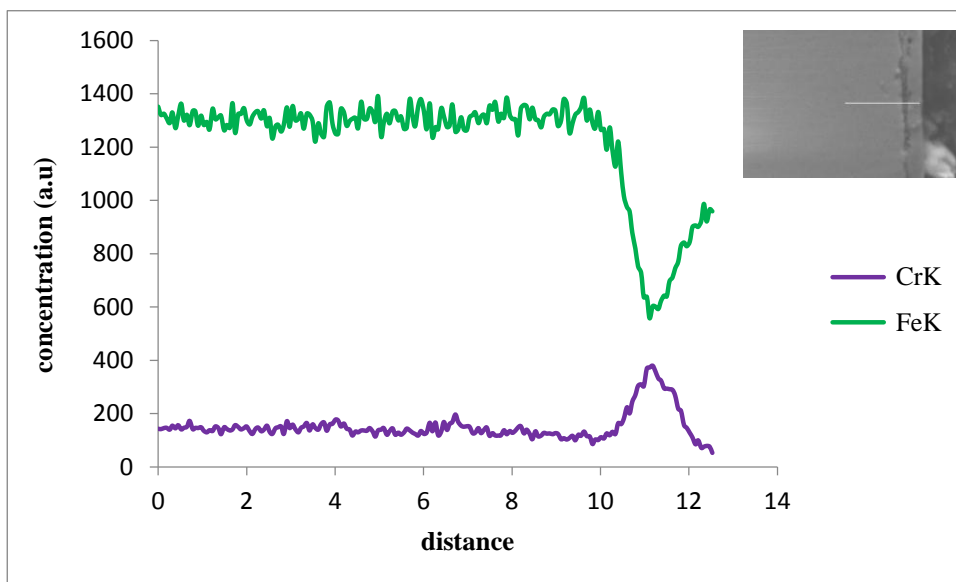
Figure 5.10 Elemental concentration profiles inside P-5 steelextending to the oxide layer formed in air at 500°C
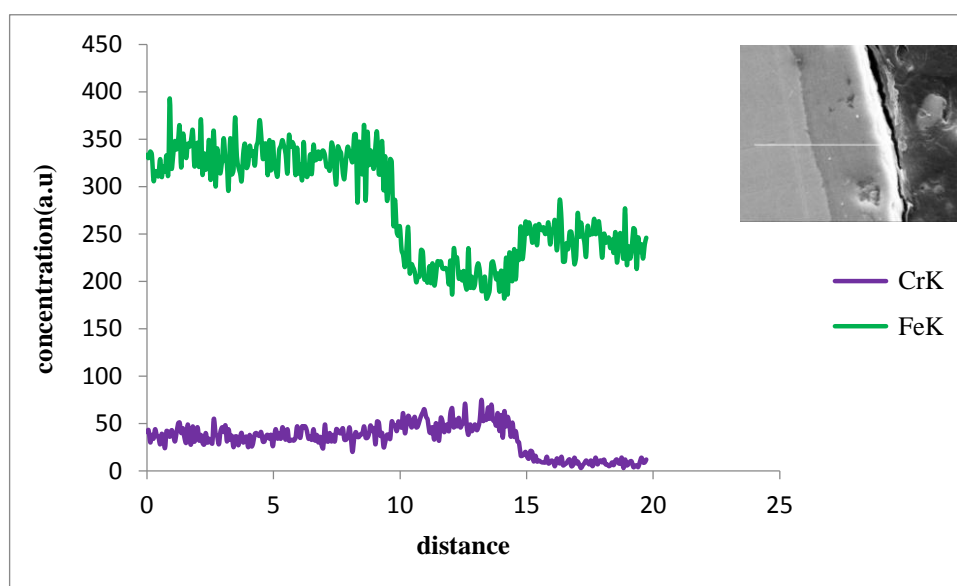
Figure 5.11 Elemental concentration profiles inside P-5 steel extending to the oxide layer formed in $CO_2+H_2O+N_2$ at $500^{o}C$

Through the literature it was found that hydrogen interferes with chromium in two ways during oxidation. In one of the ways, it was stated that part of H_2 gas resulted from the dissociation reaction of H_2O at the scale surface would diffuse in to the oxide scale as protons. Considering this mechanism, Tevten et al. [66] stated that to keep the neutrality of the oxide due to the increase in H^+ in Cr_2O_3 scale layer, chromium ion vacancies should be decreased. This led to an increase in the diffusion rate of Cr^{+3} out from Cr_2O_3 and the result was formation of oxide with lower Cr and loss of the corrosion resistance property. The other way is related to the diffusion of gaseous H_2O through the cracks in the scale to the steel surface where it reacts with metal to form oxide and hydrogen. Part of the hydrogen that is formed would permeate into the metal and results in internal oxidation as stated previously.

In the light of above mentioned discussions, it can be concluded that hydrogen available from reaction or dissociation of water was responsible for higher corrosion rates of P-5 and P-22 steels in $H_2O+CO_2+N_2$ environment. So it was possible to reduce the corrosion attack on those steels if the amount of hydrogen in the environment was reduced. Figure 4.9 shows that introducing free oxygen with water vapor resulted in decreasing the weight gain during oxidation of P-5 steel. Introduction of free oxygen could suppress water dissociation and lead to reduction of hydrogen production and the result was lower corrosion rate. Another explanation for lower weight gain when free oxygen was introduced was that free oxygen reacted with the steel forming oxide with higher Cr on the surface that could reduce the interaction between the steel and water vapor. This led to lower hydrogen diffusion in to the steel and the result was lower corrosion rate. Figure 5.11(a) shows an optical photo of the surface of P-5 steel oxidized for 30 minutes in $H_2O+N_2+O_2$ environment that has R=0.25. From this figure, two regions of different color tones labeled as 1 and 2 can be seen. On the other hand, Figure 5.11(b) shows only one region labeled as 3 when P-5 steel was oxidized in H_2O+N_2 for 30 minutes. SEM photos of regions 1, 2 and 3 shown in Figure 5.11 are given

in Figure 5.12. From this figure it can be seen that morphologies of oxides are different from one another. Figure 5.12 (a) showing region 1 has an oxide morphology that resembles or similar to the morphology of protective corundum type solid solution $(Cr,Fe)_2O_3$ found by Pujilaksono et al.[36] during oxidation of binary Fe-10Cr alloy in dry air at 600^oC. Point analysis given in Figure 5.13 shows higher Cr content of region 1 compared to regions 2 and 3 (see Figures 5.14 and 5.15). On the other hand, the oxides of regions 2 and 3 (see Figures 5.12(b) and (c)) have whiskers morphology similar to hematite scale formed during oxidation of Fe-Cr alloys [36] and pure iron [67] in wet air. The ratio between the H_2O and free oxygen concentrations (R) is an important factor as it could be seen from Figure 4.12 where breakaway of oxidation takes place at R values higher than about 2.
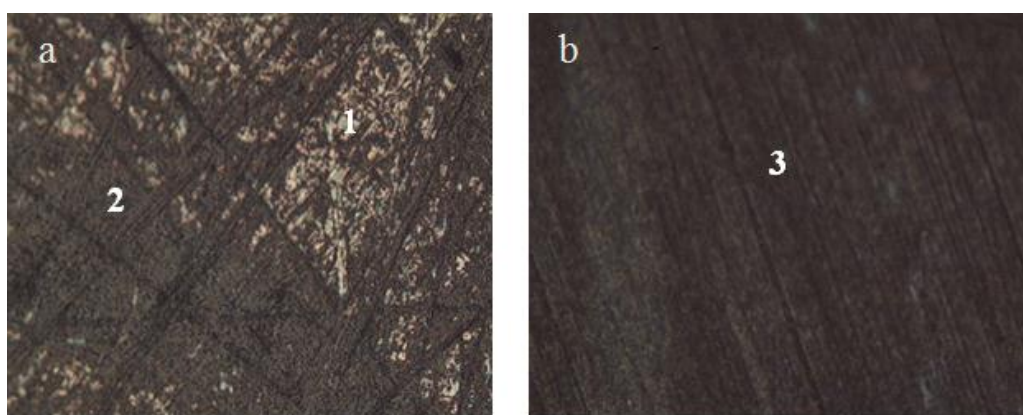
Figure 5.12 Optical surface photos of P-5 steel oxidized for 30 minutes at 500^oC in (a) $H_2O+N_2+O_2$, R=0.25 and (b) H_2O+N_2 (500X)
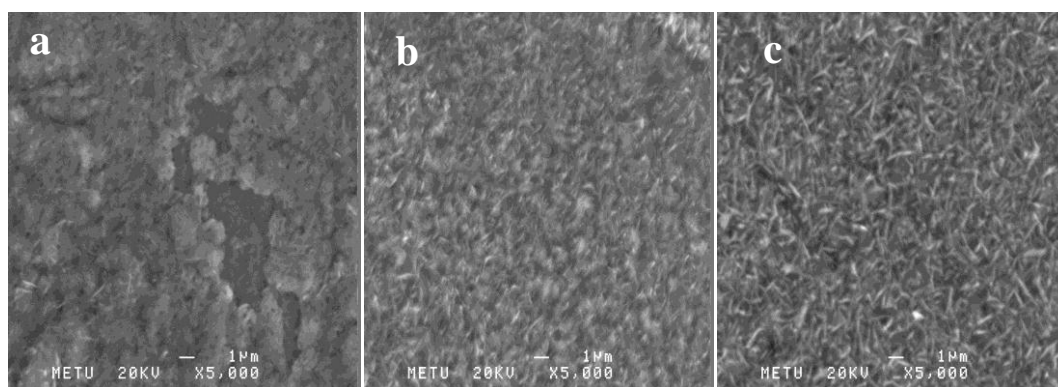
Figure 5.13 SEM images of the surface of P-5 after 30 minutes of oxidation at 500^oC (a) in $H_2O+N_2+O_2$, R=0.25, region 1, (b) in $H_2O+N_2+O_2$, R=0.25, region 2 and (c) in H_2O+N_2, region 3
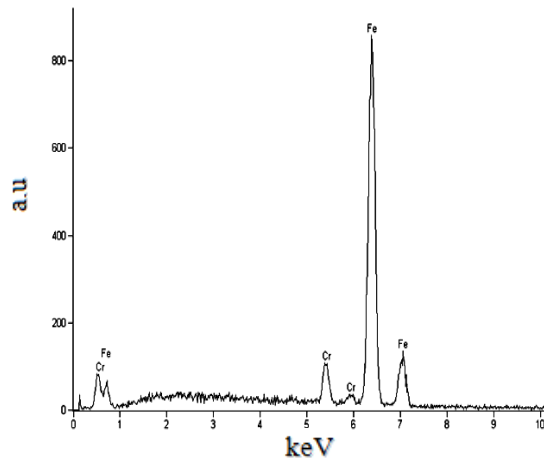
Element	Weight Conc.%	Atomic Con.%
Cr	6.24	6.67
Fe	93.76	93.33

Figure 5.14 EDS Point analysis of region 1
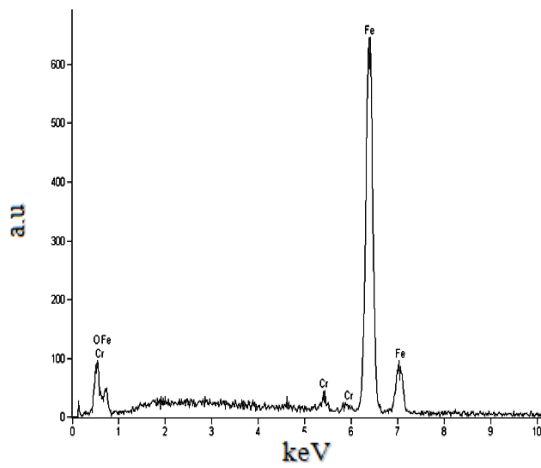
Element	Weight Conc.%	Atomic Con.%
Cr	1.77	1.89
Fe	98.23	98.11

Figure 5.15 EDS Point analysis of region 2
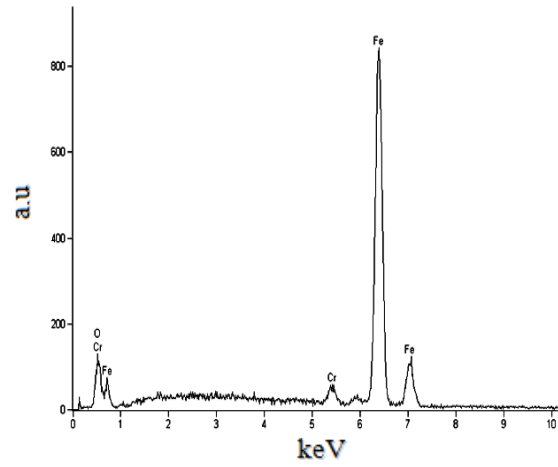
Element	Weight Conc.%	Atomic Con.%
Cr	2.80	3.00
Fe	97.20	97.00

Figure 5.16 EDS Point analysis of region 3

CHAPTER 6

CONCLUSIONS

Conclusions

According to the thermogravimetric results and analyzes discussed the following points were derived:

- Formation of an oxide layer rich in chromium on the steel surfaces made P-5 and P-22 steels gain lower weight during oxidation by air and posses higher corrosion resistance.

- In $CO_2+N_2+H_2O$ environment, C-5 retained better resistance to oxidation than P-5 and P-22. The higher oxidation rates of P-5 and P-22 in $CO_2+N_2+H_2O$ environment was attributed to the lost of protective effect of chromium due to internal oxidation.

- Although the oxygen potential was higher in the air, the oxidation rate was higher in $CO_2+N_2+H_2O$ atmosphere. This was due to formation of gaps at the metal/oxide interface and channels within the oxide phase as well as internal oxidation that promoted oxidation.

- The corrosive effect of water vapor was higher than carbon dioxide. This higher corrosivity is due to hydrogen production through reaction and/or dissociation during oxidation of steel.

- The corrosion rate could be reduced by introducing free oxygen to water vapor containing environment and decrease water vapor to oxygen partial pressures ratio in the gas phase.

- It was observed that all steels oxidized according to a parabolic equation in all oxidation tests. This supports the diffusion controlled nature of reactions.

- Oxidation rate increased with increasing temperature from $450^{o}C$ to $500^{o}C$ indicated increased diffusion with increase in temperature.

Original contributions

- Corrosion and kinetic data for low chromium content steels were collected at 450 and 500°C. The studies on high temperature oxidation of these steels especially in water vapor containing environments were not done before.

- The effect of water vapor during oxidation of low chromium steels was formalized and a mechanism was proposed by exploring the changes that takes place during oxidation.

- The passivation of low chromium steels were obtained to some extent by modifying the gas composition. It was shown that a compromise between cost of using excess air and material could be made to optimize the operations.

Suggestions for Future work

- Analytical rate equations were determined from the results of tests conducted for 48 hours, these equations could be tested when longer durations are used for the oxidation tests. The extrapolation of such results could yield a more realistic representation of real service life.

- Alloying elements have different effects on the oxidation behavior of steels so, it is suggested to use binary Fe-Cr steels with the same chromium content used in this study to eliminate the effects of other elements and collect information on the effect Cr alone. This could be repeated for other elements to develop a model to determine rates of oxidation of any steel without performing an experiment.

- Higher chromium content steels should be tested to find the minimum Cr content for external protective oxide formation in moist atmospheres.

REFERENCES

[1] F.Halliday, The Middle East in International Relations: Power and Ideology. Cambridge University Pres: USA, 270.

[2] J.H.Gary, and G.E. Handwerk, (1984). Petroleum Refining Technology and Economics (2nd Edition ed.). Marcel Dekker, Inc. ISBN 0-8247-7150-8.

[3] W.L. Leffler, (1985). Petroleum refining for the nontechnical person (2nd Edition ed.). PennWell Books.ISBN 0-87814-280-0.

[4] China Ogpe, www.China-ogpe.com,last accessed: May 2013.

[5] Corrosion Costs and Preventive Strategies in the United States, a publication of NACE International.

[6] R.D. Kane, Corrosion in Petroleum Refining and Petrochemical Operations, Corrosion: Environments and Industries, ASM Handbook, ASM International, Vol 13C, (2006), 967–1014.

[7] R.Y. Chen and W.Y.D. Yuen, Oxidation of Metals, 59, Nos. 5/6, June (2003).

[8] Yao-Nan Chang, J. Mate. Sci., 24, (1989), 14-22.

[9] W.E. Boggs and R.H. Kachik, J. Electrochem. Soc., 116, (1969), 424.

[10] D. Caplan, G. I. Speoule, R.J Hussey and M.J. Graham, Oxid. Met., 12, (1978).

[11] Idem, ibid, 13, (1973), 225.

[12] A.U. Malik and D.P. Whittle, Oxid. Met., 16, (1981), 339.

[13] Gerald H. Meier , Keeyoung Jung ,Nan Mu , Nazik M. Yanar , Frederick S. Pettit , J. Piron Abellan,Tomasz Olszewski, L.Nieto Hierro, Willem J. Quadakkers, Gordon R. Holcomb, Oxid. Met., 74, (2010), 319–340.

[14] A. M. Huntz, V. Bague, G. Beauple, C. Haut, C. Severac, P. Lecour, X. Longaygue, and F. Ropital,Applied Surface Science, 207, 255 (2003).

[15] F. Saequsa and L. Lee, Corrosion, 22, (1966), 168.

[16] J. Zurek, E. Wessel, L. Niewolak, F. Schmitz, T.-U. Kern, L.Singheiser, W.J. Quadakkers, Corrosion Science, 46, (2004), 2301–2317.

[17] Y. Inkuchi and Y. Ito. Bull., Jpn. Inst. Met., 23, (1984), 276.

[18] V. Lepingle, G. Louis, D. Petelot, B. Lefebvre, J.C. Vaillant, in:Proceedings EUROCORR 2000, 10–14 September, London, UK,2000.

[19] M. Schutze, S. Renusch, M. Schorr, Corrosion Engineering Science and Technology 39 (2) (2004) 157–166.

[20] G.G. Brown, K.G.Wold, JISI, 207, (1969), 1457.

[21] Papp, John F. "Mineral Yearbook 2002: Chromium". United States Geological Survey. Retrieved 2009-02-16.

[22] http://www.crct.polymtl.ca/FACT/documentation/SGnucl/SGnucl_Figs.htm, last accessed: August 2013

[23] P. Kofstad and K.P. Lillerud; J. Electrochem. Soc., 127 (1980) 2410

[24] P. Kofstad, K.P. Lillerud; Oxid. Met., 17 (1982) 177

[25] J. Ehlers, D. J. Young, E. J. Smaardijk, A. K. Tyagi, H. J.Penkalla, L. Singheiser,

W. J. Quadakkers, Corros. Sci. 48,(2006), 3428.

[26] C. S. Tedmon, J. Electrochem. Soc. 113, (1966), 766.

[27] A. Rahmel, J. Tobolski, Corros. Sci., 5, (1965), 333.

[28] A. Galerie, Y. Wouters, M. Caillet, Mater. Sci. Forum, 231, (2001), 369–372,.

[29] M. Schütze, D. Renusch, M. Schorr, Corros. Eng., Sci. Technol., 39, (2004), 157.

[30] M. Thiele, H. Teichmann, W. Schwarz, W. J. Quadakkers, VGB Kraftwerkstechnik.,2, (1997), 77.

[31] H. Asteman, J.-E. Svensson, L.-G. Johansson, M. Norell, Oxid. Met., 52, (1999), 95.

[32] H. Asteman, J.-E. Svensson, L.-G. Johansson, M. Norell, Oxid. Met., 54,(2000), 11.

[33] S. Henry, A. Galerie, L. Antoni, Mater. Sci. Forum,352,(2001), 369.

[34] A. Sultan, I. Karakaya, M. Erdoğan, Mater. and Corr., 63, (2012), 119

[35] A. Essuman, G. H. Meier, J. Zurek, M. Hansel, W. J.Quadakkers, Oxid. Met., 69, (2008), 143.

[36] B. Pujilaksono , T. Jonsson , H. Heidari,M. Halvarsson , J.-E. Svensson ,

L.-G. Johansson,Oxid.Met., 75, (2011), 183–207.

[37] C. T. Fujii, R. A. Meussner, J. Electrochem. Soc., 111,(1964), 1215.

[38] S. Jianian, Z. Longjiang, L. Tiefan, Oxid. Met., 48, (1997), 347.

[39] A. Holt, P. Kofstad, Solid State Ionics, 69, (1994), 137.

[40] A. S. Khanna, P. Kofstad, presented at International Conference on Microscopy of Oxidation, London, England, (1990), 113.

[41] S. R. J. Saunders, M. Monteiro, and F. Rizzo, Progress in Materials Science, 53, (2008), 775-837

[42] H. C. Graham, and H. H. Davies, American Ceramic Society, 54, (1971), 89–93.

[43] C. A. Stearns, F. J. Kohl, and G. C. Fryburg, Electrochemical Society, 121, (1974), 945–951 .

[44] E. J. Opila, D. L. Myers, N. S. Jacobson, I. M. B. Nielsen, D. F. Johnson, J. K. Olminsky, M. D. Allendorf, J. Phys. Chem., 111, (2007), 1971

[45] H. Asteman, J.E. Svensson, L.G. Johansson, Oxid. Met., 57, (2002), 193

[46] D. Caplan and M. Cohen; J. Electrochem. Soc., 108, (1961), 438

[47] A. Yamauchi, K. Kurokawa and H. Takahashi, Oxid. Met., 59, (2003), 517

[48] M. Hänsel, Diss. RWTH Aachen, Jül-3583, September 1998, ISSN0944-2952

[49] M. Ueda, M. Nanko, K. Kawamura, T. Maruyama, Mater. High Temp., 20, (2003), 109.

[50] K. Nakagawa, Y. Matsunaga, T. Yanagisawa, Mater.High Temp., 20, (2003), 67.

[51] Z. Yang, M.S. Walker, P. Singh, J.W. Stevenson, Electrochem.Solid State Lett., 6, (2003), 35.

[52] N. Mu, K. Jung, N. M. Yanar, F. S. Pettit, G. R. Holcomb, B. H. Howard, G. H. Meier, Oxid. Met., DOI 10.1007/s11085-012-9349-8, 2013

[53] A. R. Setiawan, M. Hanafi Bin Ani, M. Ueda, K. Kawamura and T. Maruyama, ISIJ International, 50, (2010), 259-263.

[54] M. Nakai , K. Nagai, Y. Murata, M. Morinaga, Corrosion Science, 48, (2006), 3869–3885.

[55] F. H. Stott, G. C. Wood, D. P. Whittle, B. D. Bastow, Y. Shida and A. Martinez-Villafane, Solid State Ionics,12, (1984), 365.

[56] C. S. Giggins and F. S. Pettit, Oxidation of Metals 14, (1980), 363.

[57] C. T. Fujii, R. A. Meussner, J. Electrochem. Soc., 114, (1967), 435.

[58] N. Birks, G.H. Meier, Introduction to High Temperature Oxidation of Metals, (1982), 74.

[59] Mars G. Fontana, Corrosion Engineering, McGraw-HILL, International Edition, 3rd edition (1987).

[60] P. Kofstad, High-Temperature Oxidation of Metals, John Wiley & Sons, New York, 1966.

[61] A. Sultan, High temperature corrosion of steels used in petroleum refinery heaters, M.Sc. thesis, Middle East Technical University, Ankara (2005).

[62] C.Wagner: Z. Elektroch, 63, (1959), 772.

[63] W. T. Thompson, C. W. Bale, A. D. Pelton, Facility for the Analysis of Chemical Thermodynamics (FACT), McGillUniversity Montreal, Royal Military College of Canada in,Kingston, Ecole Polytechnique, Montreal 1985.

[64] A. Rahmel, J. Tobolski, Corros. Sci., 5, (1965), 333.

[65] M. Hanafi, T. Kodama, M. Ueda, K. Kawamura and T. Maruyama:Mater. Trans., 50, (2009), 2656.

[66] B.Tevten, G.Hultiquist and T.norby, Oxid.Met., 51, (1999), 221.

[67] N. Bertrand, C. Desgranges, D. Gauvain, D. Monceau, and D. Poquillon, Materials Science Forum, 591, (2004), 461–464.

APPENDIX A

COMPOSITION TRIANGLE RAW DATA
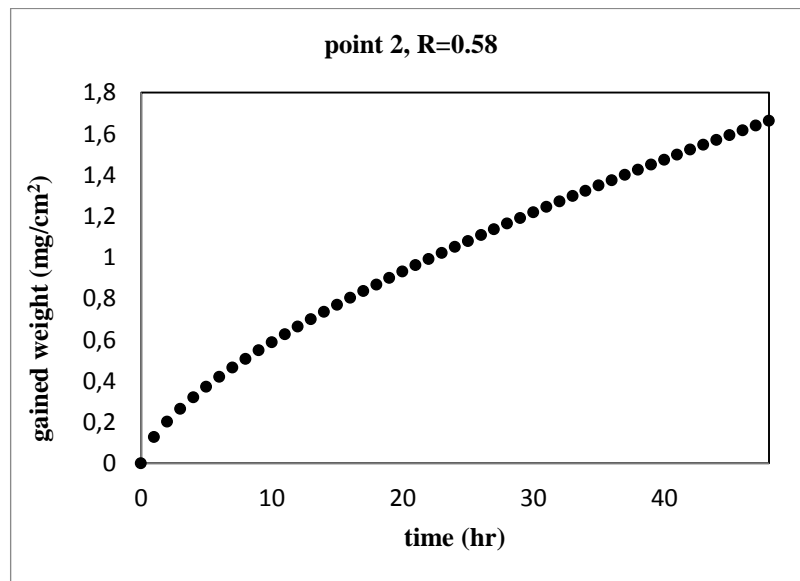
Figure A.1 Weight gain vs. time of P-5 at 500°C point 2, R=0.58
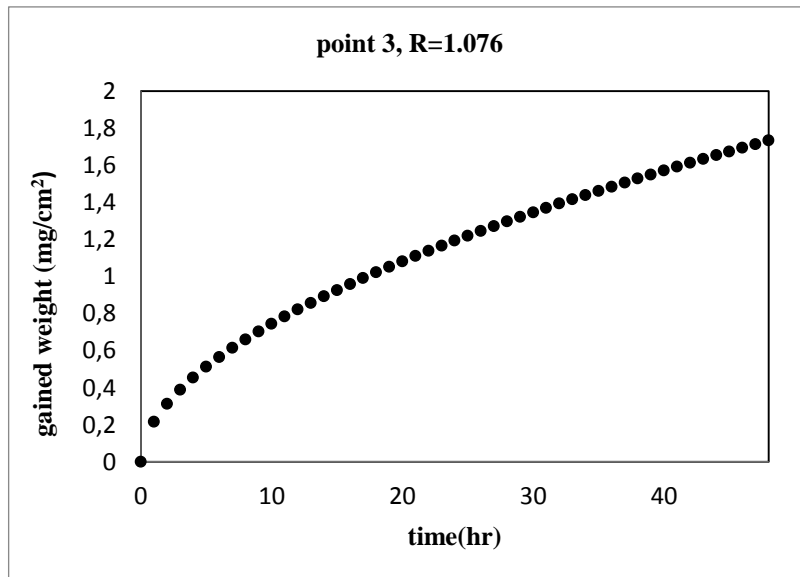
Figure A.2 Weight gain vs. time of P-5 at 500°C point 3, R=1.076
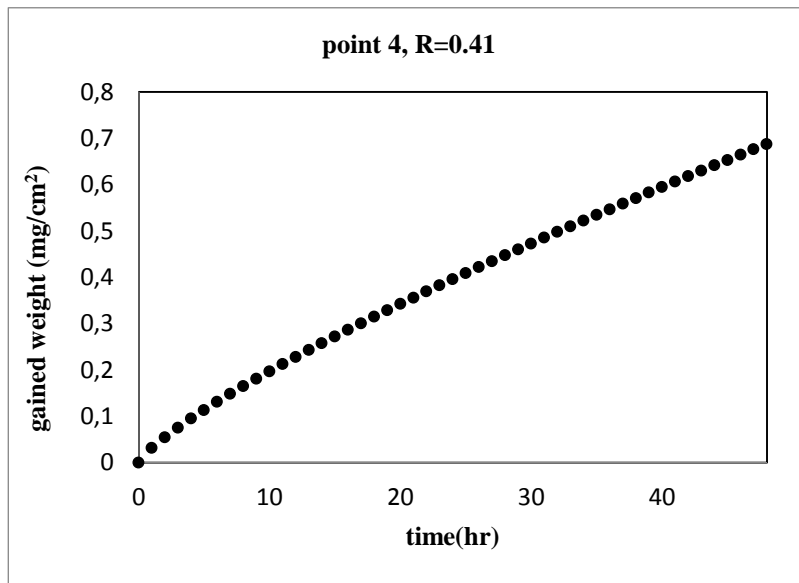
Figure A.3 Weight gain vs. time of P-5 at 500°C point 4, R=0.41
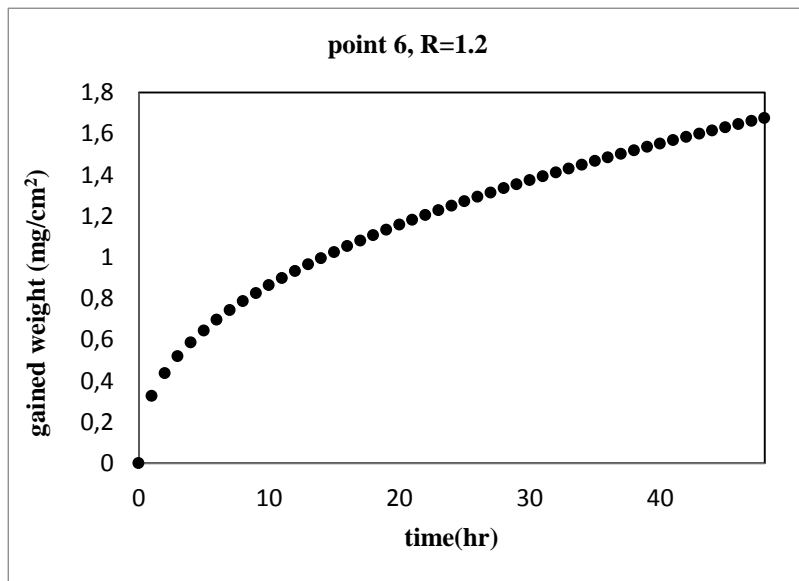
Figure A.4 Weight gain vs. time of P-5 at 500°C point 6, R=1.2
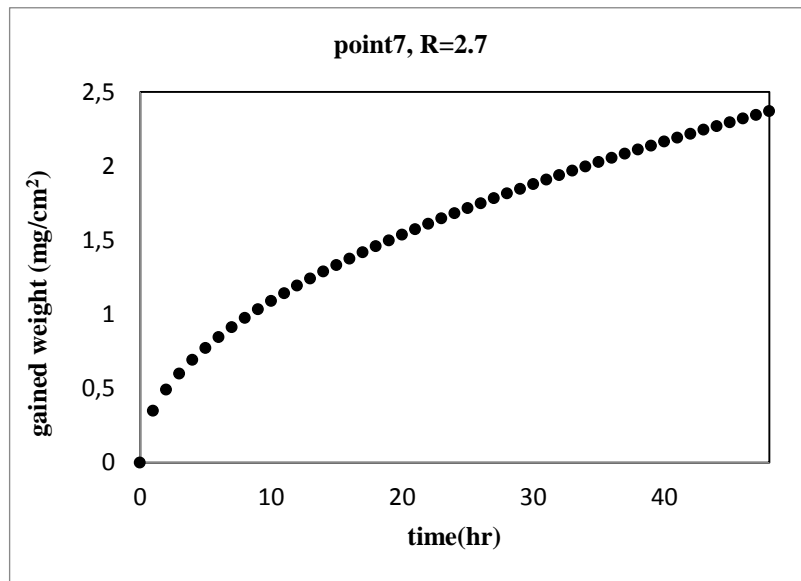
Figure A.5 Weight gain vs. time of P-5 at 500°C point 7, R=2.7
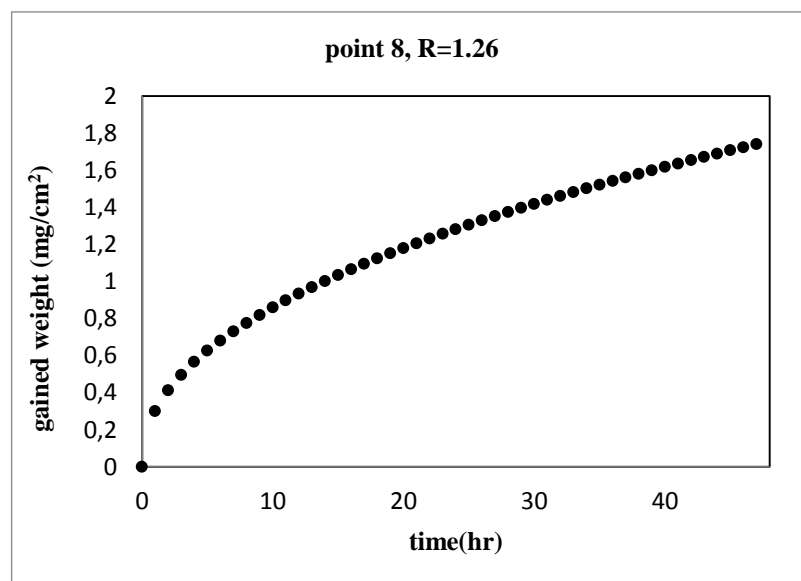
Figure A.6 Weight gain vs. time of P-5 at 500°C point8, R=1.26
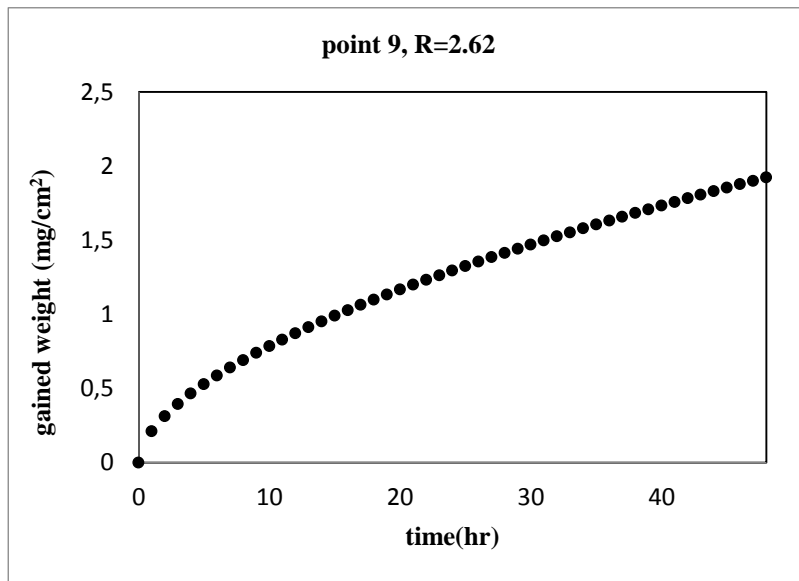
Figure A.7 Weight gain vs. time of P-5 at 500°C point 9, R=2.62
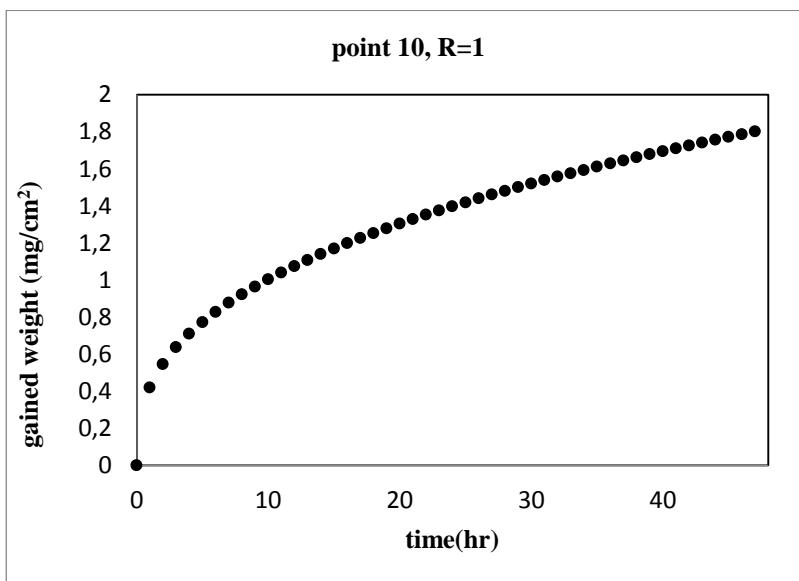
Figure A.8 Weight gain vs. time of P-5 at 500°C point 10, R=1.0

APPENDIX B

TREATMENT OF DATA

The weight gain per unit area data does not show the clear damage due to corrosion at working conditions, therefore the depth of penetration of corrosion that equivalent to 48hr oxidation period in centimeters and that equivalent to one year oxidation period in MPY was calculated for each steel sample using the parabolic rate equation and the (oxide) scale composition. Assuming that the oxides formed are Fe_2O_3 and Fe_3O_4, the Fe_2O_3 fraction $(X_{Fe_2O_3})$ was calculated from the layers observed in optical micrographs and tabulated in Table B.1. This fraction was used to calculate the relative amounts of Fe_2O_3 and Fe_3O_4.

Table B.1 Fe_2O_3 fractions for the oxidized steels

Steel	$X_{Fe_2O_3}$ (air)		$X_{Fe_2O_3}$ (H_2O)	
	450°C	500°C	450°C	500°C
C-5	0.152	0.20	0.166	0.248
P-11	0. 218	0.248	0.248	0.27
P-22	1	1	0.20	0.23
P-5	1	1	0.20	0.27

$$X_{Fe_3O4} = 1 - X_{Fe_2O_3}$$

During oxidation the weight gain recorded was the weight of O atoms that reacted with Fe atoms, so using the weight gain data and oxide fractions, the theoretical oxide scale thickness, l, in centimeters, can be calculated according to the following equation:

$$l = \frac{y}{1000*d}$$

where y is the amount of weight gain in 48 hours oxidation period in mg/cm^2 and

$$d = \left[\left(M * \frac{48}{160} * X_{Fe_2O_3}\right) + \left(N * \frac{64}{232} * (1 - X_{Fe_2O_3})\right)\right]$$

Where:

M is the density of Fe_2O_3 = 5.24 g/cm^3

N is the density of Fe_3O_4 = 5.18 g/cm^3

Then the amount of Fe converted to Fe_2O_3 and Fe_3O_4 oxides in mg/cm^2 is equal to

$$l * 5.24 * \frac{112}{160} * X_{Fe_2O_3}$$

and

$$l * 5.18 * \frac{168}{232} * (1 - X_{Fe_2O_3})$$

Dividing the summation of the above two terms (total amount of Fe oxidized to Fe_2O_3 and Fe_3O_4) by the density of pure iron (7.86g/cm^3) neglecting other elements in the steels, the theoretical depth of penetration in (cm) after 48 hours of oxidation period and that equivalent to one year oxidation in MPY (Milli inch Per Year) can be calculated and tabulated in Tables B.2 and B.3 for all steels.

Table B.2 Results of penetration depth calculation for air oxidation

Steel	Pen.depth at 450°C		Pen.depth at 500°C	
	cm in 48-hrs	MPY	cm in 48-hrs	MPY
C-5	0.000117	1.303	0.000243	1.295
P-11	0.000209	1.111	0.000281	1.492
P-22	7.45E-05	0.397	0.00017	0.904
P-5	3.95E-05	0.209	8.91E-05	0.474

Table B.3 Results of penetration depth calculation for $CO_2+N_2+H_2O$ oxidation

Steel	Pen.depth at 450^oC		Pen.depth at 500^oC	
	cm in 48-hrs	MPY	cm in 48-hrs	MPY
C-5	0.000137	0.729	0.000231	1.227
P-11	0.000188	0.999	0.000302	1.608
P-22	0.000114	0.654	0.000329	1.748
P-5	0.000305	1.622	0.000499	2.652

APPENDIX C

THERMODYNAMIC CALCULATIONS

The results of equilibrium computations using F*A*C*T (Facility for the Analysis of Chemical Thermodynamics) on-line computer program mentioned in section 5.2 are given below. Reactions of Fe with the gas phase was used to obtain the equilibrium composition of the products by Gibbs energy minimization.

Oxidation in air at 450°C

$Fe + O_2 + 3.76 N_2 =$
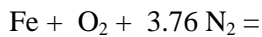
4.0100   mol   gas_ideal
(0.93766 N_2 + 6.2344E-02 O_2 + ...) (450 C, 1 atm,   a=1.0000)
.
.
+ 0.50000   mol Fe_2O_3_hematite
(79.844 gram, 0.50000 mol)
(450 C, 1 atm, S1, a=1.0000)

Oxidation in air at 500°C
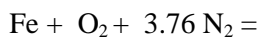
$Fe + O_2 + 3.76 N_2 =$

4.0100   mol   gas_ideal
(0.93766 N_2 + 6.2344E-02 O_2 + …) (500 C, 1 atm,   a=1.0000)
.
.
+ 0.50000   mol Fe_2O_3_hematite
(79.844 gram, 0.50000 mol)
(500 C, 1 atm, S1, a=1.0000)

Oxidation in $CO_2 + N_2$ at 450^oC

$Fe + CO_2 + 3.76 N_2 =$

4.1076   mol   gas_ideal
(0.91538 N_2 + 7.7677E-02 CO_2+ 6.9462E-03 CO) (450 C, 1 atm,   a=1.0000)

.
.
.

+ 0.65240   mol   C_graphite
(7.8358 gram, 0.65240 mol)
(450 C, 1 atm, S1, a=1.0000)

+ 0.33333   mol Fe_3O_4magnetite
(77.178 gram, 0.33333 mol)
(450 C, 1 atm, S1, a=1.0000)

+ 0   mol Fe_3O_4_magnetite
(450 C, 1 atm, S2, a=0.85764)

+ 0   mol   C_diamond
(450 C, 1 atm, S2, a=0.46431)

+ 0   mol   FeO_wustite
(450 C, 1 atm, S1, a=0.38106)

+ 0   mol   Fe_bcc
(450 C, 1 atm, S1, a=5.4062E-02)

+ 0   mol   Fe_fcc
(450 C, 1 atm, S2, a=3.9440E-02)

+ 0   mol Fe_2O_3_hematite
(450 C, 1 atm, S1, a=3.9165E-02)

+ 0   mol   FeO_liquid
(450 C, 1 atm, L1, a=2.0847E-02)

+ 0   mol   Fe_liquid
(450 C, 1 atm, L1, a=1.0581E-02)

Oxidation in $CO_2 + N_2$ at 500^oC

Fe + CO2 + 3.76 N$_2$ =

4.1283   mol   gas_ideal
 (0.91078 N$_2$+ 7.2261E-02 CO$_2$ + 1.6963E-02 CO) (500 C, 1 atm,   a=1.0000)

.
.
+ 0.63165   mol   C_graphite
(7.5866 gram, 0.63165 mol)
(500 C, 1 atm, S1, a=1.0000)

+ 0.33333   mol   Fe$_3$O$_4$_magnetite
(77.178 gram, 0.33333 mol)
(500 C, 1 atm, S1, a=1.0000)

+ 0   mol   Fe$_3$O$_4$_magnetite
(500 C, 1 atm, S2, a=0.93902)

+ 0   mol   FeO_wustite
(500 C, 1 atm, S1, a=0.58109)

+ 0   mol   C_diamond
(500 C, 1 atm, S2, a=0.47183)

+ 0   mol   Fe_bcc
(500 C, 1 atm, S1, a=0.17235)

+ 0   mol   Fe_fcc
(500 C, 1 atm, S2, a=0.13551)

+ 0   mol   FeO_liquid
(500 C, 1 atm, L1, a=4.4462E-02)

+ 0   mol   Fe_liquid
(500 C, 1 atm, L1, a=4.1814E-02)

+ 0   mol   Fe$_2$O$_3$_hematite
(500 C, 1 atm, S1, a=3.2187E-02)

+ 0   mol   Fe$_3$C_cementite
(500 C, 1 atm, S1, a=1.4938E-03)

Oxidation in CO_2+H_2O at 450°C

Fe + CO_2 + 2 H_2O =

2.5330   mol gas_ideal
(0.45946 H_2O + 0.29072 CO_2 + 0.14574 H_2 + 9.2193E-02 CH_4 + 1.1880E-02 CO) (450 C, 1 atm, a=1.0000)
.
.
.
+ 0.33333   mol Fe_3O_4_magnetite
(77.178 gram, 0.33333 mol)
(450 C, 1 atm, S1, a=1.0000)

+ 0   mol Fe_3O_4_magnetite
(450 C, 1 atm, S2, a=0.85764)

+ 0   mol C_graphite
(450 C, 1 atm, S1, a=0.78153)

+ 0   mol C_diamond
(450 C, 1 atm, S2, a=0.36288)

+ 0   mol FeO_wustite
(450 C, 1 atm, S1, a=0.29351)

+ 0   mol Fe_2O_3_hematite
(450 C, 1 atm, S1, a=5.0848E-02)

+ 0   mol Fe_bcc
(450 C, 1 atm, S1, a=1.9028E-02)

+ 0   mol FeO_liquid
(450 C, 1 atm, L1, a=1.6058E-02)

+ 0   mol Fe_fcc
(450 C, 1 atm, S2, a=1.3882E-02)

+ 0   mol Fe_liquid
(450 C, 1 atm, L1, a=3.7243E-03)

Oxidation in CO_2+H_2O at 500^oC

Fe + CO_2 + 2 H_2O =
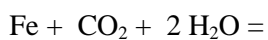
2.6484   mol gas_ideal
 (0.41230 H_2O + 0.28340 CO_2 + 0.21011 H_2 + 6.6383E-02 CH_4 + 2.7810E-02 CO) (500 C, 1 atm,   a=1.0000)
.

.

.
+ 0.33333   mol Fe_3O_4_magnetite
(77.178 gram, 0.33333 mol)
(500 C, 1 atm, S1, a=1.0000)

+ 0   mol Fe_3O_4_magnetite
(500 C, 1 atm, S2, a=0.93902)

+ 0   mol   C_graphite
(500 C, 1 atm, S1, a=0.68532)

+ 0   mol   FeO_wustite
(500 C, 1 atm, S1, a=0.43449)

+ 0   mol   C_diamond
(500 C, 1 atm, S2, a=0.32336)

+ 0   mol   Fe_bcc
(500 C, 1 atm, S1, a=5.3869E-02)

+ 0   mol Fe_2O_3_hematite
(500 C, 1 atm, S1, a=4.3047E-02)

+ 0   mol   Fe_fcc
(500 C, 1 atm, S2, a=4.2356E-02)

+ 0   mol   FeO_liquid
(500 C, 1 atm, L1, a=3.3245E-02)

+ 0   mol   Fe_liquid
(500 C, 1 atm, L1, a=1.3070E-02)

CURRICULUM VITAE

PERSONAL INFORMATION

Surname, Name: Sultan, Abdelrahman

Nationality: Libyan

Date and Place of Birth: 3 August 1970, Libya

Marital Status: Married

Phone: +90 506 492 61 16

email: e135351@metu.edu.tr OR sultanabdelrahman@yahoo.com

EDUCATION

Degree	Institution	Year of Graduation
MS METU	Metallurgical and Materials Engineering	2005
BS	Alfatih university Chemical Engineering	1994
High School	Souk Hameis High School, Libya	1988

WORK EXPERIENCE

Year	Place	Enrollment
2005-2008	Almergeb University Department of Chemical Engineering	Lecturer
1999-2001	Central institute of construction materials control	Quality Control Engineer
1995-2001	Almergeb University Department of Chemical Engineering	Research Assistant

FOREIGN LANGUAGES

Advanced English (writing and speaking), Turkish (speaking)

PUBLICATIONS

1. A. Sultan, İ. Karakaya and M. Erdoğan, INFLUENCE OF WATER VAPOR ON HIGH TEMPERATURE OXIDATION OF STEELS USED IN PETROLEUM REFINERY HEATERS, "Materials and Corrosion", 63, 2 (2012) 119–126.

2. Abdelrahman SULTAN, Ishak KARAKAYA, Metehan ERDOGAN, COMPARISON OF BEHAVIOURS OF LOW CHROMIUM STEELS IN AIR AND MOIST ATMOSPHERES AT HIGH TEMPERATURES, in EuroCorr 2012, p1230/1-10, The European Corrosion Congress, İstanbul 2012, European Federation of Corrosion Event No. 330.

3. A. Sultan, İ. Karakaya, M. Erdoğan, Petrol Rafinerilerinin Isıtıcılarında Kullanılan Çeliklerin Yüksek Sıcaklıkta Oksitlenmeleri, "Korozyon", 17(1-2), (2009), s.22-28.

4. A. Sultan, İ. Karakaya, M. Erdoğan, Petrol Rafinerilerinin Isıtıcılarında Kullanılan Çeliklerin Yüksek Sıcaklıkta Oksitlenmeleri, "KORSEM'08 XI. Uluslararası Korozyon Sempozyumu", Korozyon Derneği, İzmir 2008, p.384-393.